

# The effect of interfacial pressure in the discrete-equation multiphase model

Svend Tollak Munkejord <sup>a,\*</sup> and Mikael Papin <sup>b,1</sup>

<sup>a</sup>*Norwegian University of Science and Technology (NTNU),  
Department of Energy and Process Engineering,  
Kolbjørn Hejes veg 1A, NO-7491 Trondheim, Norway*

<sup>b</sup>*Bordeaux 1 University, Department of Applied Mathematics,  
351 Cours de la Libération, FR-33405 Talence cedex, France*

---

## Abstract

Abgrall and Saurel [1] presented a discrete-equation two-pressure two-phase model of seven equations. A main characteristic of that model is that the Riemann problems are solved between two pure fluids, and that phase interaction is determined by the Riemann solver. Here we propose a five-equation isentropic simplification of the discrete-equation model, and by examples we show how existing and new models for interfacial closures can be incorporated into it. The interfacial pressure has a determining effect on the final solution. We further show that the discrete-equation model can reproduce results for two-phase shock tubes given in the literature when the adequate interfacial-pressure model is employed. Finally, we compare the present results with those of a continuous five-equation model, and obtain very good agreement.

*Key words:* Discrete multiphase model, interfacial pressure, two-phase flow, compressible flow, pressure relaxation.

---

---

\* Corresponding author

*Email addresses:* [stm@pvv.ntnu.no](mailto:stm@pvv.ntnu.no) (Svend Tollak Munkejord),  
[mikael.papin@neuf.fr](mailto:mikael.papin@neuf.fr) (Mikael Papin).

*URL:* <http://www.pvv.ntnu.no/~stm/dring/> (Svend Tollak Munkejord).

<sup>1</sup> Current address: INRIA Futurs, projet Scalaplix; LaBRI, 351 Cours de la Libération, FR-33405 Talence cedex, France

# 1 Introduction

## 1.1 Background

Multiphase flows are relevant in a large and increasing amount of applications, including in the oil and gas industries, in the chemical and process industries, in heat pumping applications, and in nuclear power plants. Still, the mathematical modelling and numerical simulation of multiphase flows is, as a whole, not a mature science. Only in specialized areas is the state of the art satisfactory.

In the present paper, we focus on two-phase flows. In recent years, progress has been made regarding the understanding of the mathematical properties and the proper spatial discretization of two-phase models. However, these questions are challenging, and hence, in the research papers presented, one has often not been able to attend to the constitutive terms in need of physical modelling and experimental verification.

Here we investigate ways to model the interfacial pressure in the framework of the discrete-equation model of Abgrall and Saurel [1].

## 1.2 Previous work

Saurel and Abgrall [14] presented a two-velocity two-pressure two-phase model of seven equations, where pressure and / or velocity relaxation could be performed after the hyperbolic time step. The model was expanded to several space dimensions by Saurel and LeMetayer [15], and it was stated to be suitable for compressible multiphase flows with interfaces, shocks, detonation waves and cavitation.

The approximate Riemann solver employed by Saurel and Abgrall [14] was a modified Harten, Lax, and van Leer (HLL) scheme. Other authors have later presented similar methods using other solvers. Niu [12] applied a modified advection upstream splitting method (AUSMD) and solved the seven-equation model in one and two dimensions, also adding a  $k$ - $\varepsilon$  turbulence model. A Roe-type scheme for the seven-equation model was presented by Karni *et al.* [7].

One of the main difficulties of the above-mentioned two-phase model, is the occurrence of non-conservative products. Abgrall and Saurel [1] proposed a discrete-equation two-phase model aiming to avoid the problems of the non-conservative terms by considering Riemann problems between

pure phases. This approach leads to the phase interaction being defined through the Riemann solver.

### 1.3 Outline of paper

The present paper analyses the interfacial pressure and the discrete-equation model. Section 2 briefly presents the multiphase model. The discrete-equation numerical scheme of Abgrall and Saurel [1] is revisited in Section 3. Furthermore, similarities to, and differences from, the continuous model are pointed out, and the pure-phase Riemann problem is explained. The continuous model used for comparisons is briefly referred to in Section 4. Test calculations are presented in Section 5, and conclusions are drawn in Section 6.

## 2 Multiphase model

The one-dimensional, inviscid, isentropic multiphase flow is customarily described by the continuity equation

$$\frac{\partial}{\partial t}(\alpha^{(k)}\rho^{(k)}) + \frac{\partial}{\partial x}(\alpha^{(k)}\rho^{(k)}u^{(k)}) = 0, \quad (1)$$

and the momentum equation

$$\frac{\partial}{\partial t}(\alpha^{(k)}\rho^{(k)}u^{(k)}) + \frac{\partial}{\partial x}(\alpha^{(k)}\rho^{(k)}(u^{(k)})^2) + \alpha^{(k)}\frac{\partial p^{(k)}}{\partial x} + (p^{(k)} - p_{\text{int}}^{(k)})\frac{\partial \alpha^{(k)}}{\partial x} = 0, \quad (2)$$

when gravity, mass transfer, wall friction, interface friction, and other effects are neglected. This model is arrived at by volume-averaging the governing equations for each phase, and by considering a cross-section of a pipe. Due to the term  $p_{\text{int}}^{(k)}\partial\alpha^{(k)}/\partial x$ , the equation system cannot be written in conservative form. The Riemann problem for non-conservative systems is not always unique, and it is in general difficult to define its solution [2].

A discrete mathematical and numerical model for compressible multiphase flows was introduced by Abgrall and Saurel [1]. Since the two-phase mixture was considered at the discrete, pure-phase level, the problem of the  $\nabla\alpha$  terms, which render the system of equations non-conservative [14], was avoided. For the sake of clarification, the main elements of the Abgrall and Saurel [1] model are given here in detail. Further, we adapt their model to isentropic problems, something which represents a simplification.

## 2.1 Transport equations

For an inviscid, isentropic flow, each pure fluid  $k$  is governed by the (is-entropic) Euler equations:

$$\frac{\partial \mathbf{q}^{(k)}}{\partial t} + \nabla \cdot \mathbf{F}^{(k)} = 0, \quad (3)$$

where  $\mathbf{q}^{(k)}$  is the vector containing the ‘conservative’ variables,

$$\mathbf{q}^{(k)} = \left[ \rho^{(k)}, \rho^{(k)} \mathbf{u}^{(k)} \right]^T, \quad (4)$$

and  $\mathbf{F}^{(k)}$  is the corresponding flux matrix:

$$\mathbf{F}^{(k)} = \left[ \rho^{(k)} \mathbf{u}^{(k)}, \rho^{(k)} \mathbf{u}^{(k)} \otimes \mathbf{u}^{(k)} + p^{(k)} \mathbf{I} \right]^T. \quad (5)$$

Denote the phase-indicator function (characteristic function) for phase  $k$  as  $X^{(k)}$ . It is equal to one inside phase  $k$  and zero otherwise. It is obvious that phase  $k$  is advected with the velocity of phase  $k$ . Hence the same is true for the phase-indicator function, which gives

$$\frac{\partial X^{(k)}}{\partial t} + \mathbf{u}^{(k)} \cdot \nabla X^{(k)} = 0. \quad (6)$$

$\nabla X^{(k)} = 0$ , except at the interface of phase  $k$ . Therefore it is natural to write

$$\frac{\partial X^{(k)}}{\partial t} + \mathbf{u}_{\text{int}}^{(k)} \cdot \nabla X^{(k)} = 0, \quad (7)$$

where  $\mathbf{u}_{\text{int}}^{(k)}$  is the interface velocity of phase  $k$ . The above equation is derived in detail by Drew and Passman [5, Section 9.1.3]. For two phases, we have  $\mathbf{u}_{\text{int}}^{(1)} = \mathbf{u}_{\text{int}}^{(2)} = \mathbf{u}_{\text{int}}$ .

Here we follow the ensemble-averaging approach of Drew and Passman [5, see Section 9.1 and Chapter 11]. The ensemble-averaging operator,  $\mathcal{E}(\cdot)$ , is assumed to commute with differentiation in space and time, so that

$$\mathcal{E}(\nabla \psi) = \nabla \mathcal{E}(\psi), \quad (8)$$

and

$$\mathcal{E}\left(\frac{\partial \psi}{\partial t}\right) = \frac{\partial}{\partial t} \mathcal{E}(\psi), \quad (9)$$

where  $\psi$  is a general function. Further, we have, for example

$$\int \mathcal{E}(\psi) \, dx \, dt = \mathcal{E}\left(\int \psi \, dx \, dt\right). \quad (10)$$

Drew and Passman [5] derived a relation for the ensemble average of the gradient (or divergence) of a general function  $\psi$ :

$$\mathcal{E} \left( X^{(k)} \nabla \psi \right) = \nabla \left( \mathcal{E} \left( X^{(k)} \psi \right) \right) - \mathcal{E} \left( \psi_{\text{int}}^{(k)} \nabla X^{(k)} \right), \quad (11)$$

which is similar to the Slattery averaging theorem [16, 19] for volume averaging. The subscript ‘int’ denotes the value at the interface, which is ‘picked up’ by the  $\nabla X^{(k)}$  operator.

The expression for the ensemble average of a time derivative is

$$\mathcal{E} \left( X^{(k)} \frac{\partial \psi}{\partial t} \right) = \frac{\partial}{\partial t} \left( \mathcal{E} \left( X^{(k)} \psi \right) \right) - \mathcal{E} \left( \psi_{\text{int}}^{(k)} \frac{\partial X^{(k)}}{\partial t} \right). \quad (12)$$

Thus we can write the averaged balance equations for each phase as

$$\frac{\partial \mathcal{E} \left( X^{(k)} \rho^{(k)} \right)}{\partial t} + \nabla \cdot \mathcal{E} \left( X^{(k)} \rho^{(k)} \mathbf{u}^{(k)} \right) = \mathcal{E} \left( \rho^{(k)} (\mathbf{u}^{(k)} - \mathbf{u}_{\text{int}}^{(k)}) \cdot \nabla X^{(k)} \right), \quad (13)$$

and

$$\begin{aligned} \frac{\partial \mathcal{E} \left( X^{(k)} \rho^{(k)} \mathbf{u}^{(k)} \right)}{\partial t} + \nabla \cdot \left[ \mathcal{E} \left( X^{(k)} \rho^{(k)} \mathbf{u}^{(k)} \otimes \mathbf{u}^{(k)} \right) + \mathcal{E} \left( X^{(k)} \mathbf{p}^{(k)} \right) \right] = \\ \mathcal{E} \left( (\rho^{(k)} \mathbf{u}^{(k)} \otimes (\mathbf{u}^{(k)} - \mathbf{u}_{\text{int}}^{(k)}) + \mathbf{p}^{(k)} \mathbf{I}) \cdot \nabla X^{(k)} \right). \end{aligned} \quad (14)$$

Defining the volume fraction of phase  $k$  as

$$\alpha^{(k)} = \mathcal{E} \left( X^{(k)} \right), \quad (15)$$

the average density as

$$\bar{\rho}^{(k)} = \frac{\mathcal{E} \left( X^{(k)} \rho^{(k)} \right)}{\alpha^{(k)}}, \quad (16)$$

the average velocity as

$$\bar{\mathbf{u}}^{(k)} = \frac{\mathcal{E} \left( X^{(k)} \rho^{(k)} \mathbf{u}^{(k)} \right)}{\alpha^{(k)} \bar{\rho}^{(k)}}, \quad (17)$$

etc., assuming

$$\mathcal{E} \left( X^{(k)} \rho^{(k)} \mathbf{u}^{(k)} \otimes \mathbf{u}^{(k)} \right) = \alpha^{(k)} \bar{\rho}^{(k)} \bar{\mathbf{u}}^{(k)} \otimes \bar{\mathbf{u}}^{(k)}, \quad (18)$$

and omitting the overline symbol for notational convenience, we get:

$$\frac{\partial \alpha^{(k)} \rho^{(k)}}{\partial t} + \nabla \cdot \left[ \alpha^{(k)} \rho^{(k)} \mathbf{u}^{(k)} \right] = \mathcal{E} \left( \rho^{(k)} (\mathbf{u}^{(k)} - \mathbf{u}_{\text{int}}^{(k)}) \cdot \nabla X^{(k)} \right), \quad (19)$$

and

$$\frac{\partial \alpha^{(k)} \rho^{(k)} \mathbf{u}^{(k)}}{\partial t} + \nabla \cdot [\alpha^{(k)} \rho^{(k)} \mathbf{u}^{(k)} \otimes \mathbf{u}^{(k)} + \alpha^{(k)} p^{(k)} \mathbf{I}] = \mathcal{E} \left( (\rho^{(k)} \mathbf{u}^{(k)} \otimes (\mathbf{u}^{(k)} - \mathbf{u}_{\text{int}}^{(k)}) + p^{(k)} \mathbf{I}) \cdot \nabla X^{(k)} \right). \quad (20)$$

Herein, the quantities on the left-hand side are averaged. The averaged topological equation is

$$\frac{\partial \alpha^{(k)}}{\partial t} + \mathcal{E} \left( \mathbf{u}_{\text{int}}^{(k)} \cdot \nabla X^{(k)} \right) = 0. \quad (21)$$

## 2.2 Thermodynamics

In the present work, the energy equation is not considered, and the following equation of state is employed:

$$p^{(k)} = (c^{(k)})^2 (\rho^{(k)} - \rho_{\circ}^{(k)}), \quad (22)$$

where the speed of sound  $c^{(k)}$  and the ‘reference density’  $\rho_{\circ}^{(k)}$  are constants for each phase. The above equation corresponds to the stiffened-gas equation of state,  $p = (\gamma - 1)\rho e - \gamma p_{\circ}$ , where  $e$  is the internal energy, if one takes  $c^2 = (\gamma - 1)e$  and  $\gamma p_{\circ} = c^2 \rho_{\circ}$ .

This equation of state (22) has been derived under the assumption of an isentropic flow. In fact, it also implies isothermal flow. This can be seen by considering the relation

$$ds = \frac{c_v}{T} dT + \left( \frac{\partial p}{\partial T} \right)_v dv, \quad (23)$$

which can be found in a thermodynamics textbook. Herein, the specific volume  $v = 1/\rho$ . Differentiating (22) with respect to  $T$  while keeping  $\rho$  constant, yields 0. At the same time, (22) has been derived under the assumption of constant entropy, or  $ds = 0$ . Therefore, Equation (23) dictates  $dT = 0$ , or isothermal flow.

Since we are interested in two-phase mixtures, pure single-phase flow has not been explicitly accounted for. This restriction is not thought to be of practical importance in most applications.

### 3 Numerical scheme

Henceforth we treat only one spatial dimension for simplicity. Consider the non-averaged balance equations (3) for each phase. They are multiplied by the phase-indicator function  $X^{(k)}$  and integrated over a control volume  $\mathcal{C}_i$  as follows:

$$\int_{\mathcal{C}_i} X^{(k)} \frac{\partial \mathbf{q}^{(k)}}{\partial t} dx + \int_{\mathcal{C}_i} X^{(k)} \nabla \cdot \mathbf{F}^{(k)} dx = 0, \quad (24)$$

or

$$\int_{\mathcal{C}_i} X^{(k)} \frac{\partial \mathbf{q}^{(k)}}{\partial t} dx + \int_{\partial[\mathcal{C}_i \cap \{X^{(k)}=1\}]} X^{(k)} \mathbf{F}^{(k)} \cdot \mathbf{n} ds = 0, \quad (25)$$

where  $\mathbf{n}$  is the outward-pointing unit normal vector. Using the commutation property (10), we can ensemble-average (24):

$$\mathcal{E} \left( \int_{\mathcal{C}_i} \left\{ \frac{\partial X^{(k)} \mathbf{q}^{(k)}}{\partial t} + \nabla \cdot (X^{(k)} \mathbf{F}^{(k)}) - \mathbf{q}^{(k)} \frac{\partial X^{(k)}}{\partial t} - \mathbf{F}^{(k)} \cdot \nabla X^{(k)} \right\} dx \right) = 0, \quad (26)$$

and using (7), to obtain, analogously to (19) and (20):

$$\int_{\mathcal{C}_i} \frac{\partial \alpha^{(k)} \mathbf{q}^{(k)}}{\partial t} dx + \int_{\mathcal{C}_i} \nabla \cdot (\alpha^{(k)} \mathbf{F}^{(k)}) dx = \int_{\mathcal{C}_i} \mathcal{E}(\mathbf{s}^{(k)}) dx, \quad (27)$$

where

$$\mathbf{s}^{(k)} = \begin{bmatrix} \rho^{(k)} (\mathbf{u}^{(k)} - \mathbf{u}_{\text{int}}^{(k)}) \cdot \nabla X^{(k)} \\ (\rho^{(k)} \mathbf{u}^{(k)} \otimes (\mathbf{u}^{(k)} - \mathbf{u}_{\text{int}}^{(k)}) + p^{(k)} \mathbf{I}) \cdot \nabla X^{(k)} \end{bmatrix}. \quad (28)$$

However, the topological equation (7) cannot be written in the form (3), and must therefore be treated differently. Still, we may integrate it,

$$\int_{\mathcal{C}_i} \frac{\partial X^{(k)}}{\partial t} dx + \int_{\mathcal{C}_i} \mathbf{u}_{\text{int}}^{(k)} \cdot \nabla X^{(k)} dx, \quad (29)$$

and take the ensemble average:

$$\int_{\mathcal{C}_i} \frac{\partial \mathcal{E}(X^{(k)})}{\partial t} dx = - \int_{\mathcal{C}_i} \mathcal{E}(\mathbf{u}_{\text{int}}^{(k)} \cdot \nabla X^{(k)}) dx. \quad (30)$$

Since we consider a two-phase flow at the discrete level,  $\mathcal{E}(X^{(k)}) = X^{(k)} = 1$  inside phase  $k$  and 0 otherwise, and the above equation reads  $0 = 0$  except at the interface, where the *size* of the jump in  $X^{(k)}$  equals 1.

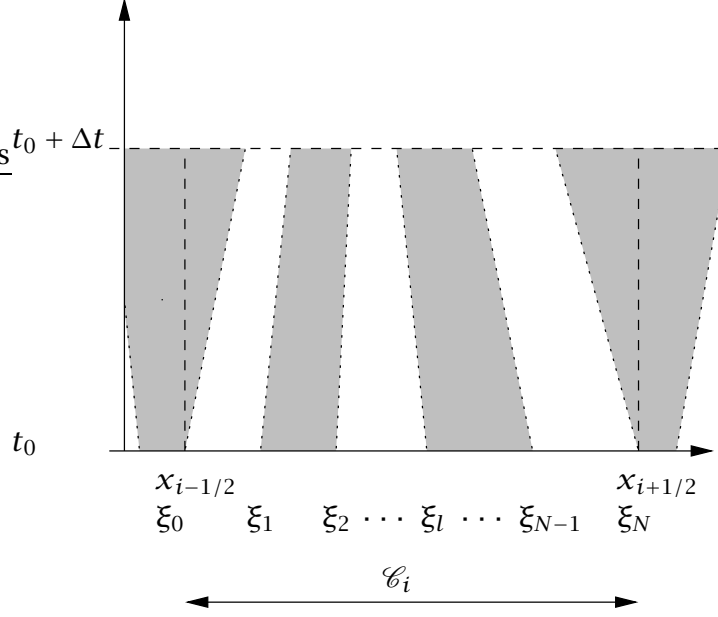


Figure 1. Space-time control volume.

### 3.1 Lagrangian fluxes

The right-hand sides of (27) and (30) give rise to the Lagrangian fluxes  $\mathbf{F}^{\text{lag},(k)}$  treated in Abgrall and Saurel [1]. They are sometimes called transfer integrals in the multiphase literature. For example, in 1D we have

$$\mathbf{S}^{(k)} = \mathbf{F}^{\text{lag},(k)} \frac{\partial X^{(k)}}{\partial x}, \quad (31)$$

where

$$\mathbf{F}^{\text{lag},(k)} = \mathbf{F}^{(k)} - \mathbf{u}_{\text{int}}^{(k)} \mathbf{q}^{(k)}. \quad (32)$$

The phase velocity  $\mathbf{u}^{(k)}$  at the interface and the corresponding interface velocity  $\mathbf{u}_{\text{int}}^{(k)}$  are different if there is mass transfer between the phases. Since in the present work we assume that no interphase mass transfer takes place, we get:

$$\mathbf{S}^{(k)} = \begin{bmatrix} 0 \\ p^{(k)} \mathbf{I} \cdot \nabla X^{(k)}. \end{bmatrix}. \quad (33)$$

Integrate (27) over  $\mathcal{C}_i \times [t_0, t_0 + \Delta t]$ :

$$\iint_{\mathcal{C}_i \times [t_0, t_0 + \Delta t]} \left( \frac{\partial \alpha^{(k)} \mathbf{q}^{(k)}}{\partial t} + \frac{\partial \alpha^{(k)} \mathbf{F}^{(k)}}{\partial x} \right) dx dt = \iint_{\mathcal{C}_i \times [t_0, t_0 + \Delta t]} \mathcal{E}(\mathbf{S}^{(k)}) dx dt. \quad (34)$$

Consider the space-time control volume shown in Figure 1. The shaded areas are pure fluid  $k$ , where  $\alpha^{(k)} = X^{(k)} = 1$ , and the white areas repres-

ent the other fluid, where  $X^{(k)} = 0$ . The dashed lines at  $x_{i-1/2}$  and  $x_{i+1/2}$  are the control-volume boundaries fixed in space. The dotted lines represent the trajectories of the interfaces between the two fluids. We can use Green's theorem, and the left-hand side of (34) becomes

$$\begin{aligned} & \iint_{\mathcal{C}_i \times [t_0, t_0 + \Delta t]} \left( \frac{\partial \alpha^{(k)} \mathbf{q}^{(k)}}{\partial t} + \frac{\partial \alpha^{(k)} \mathbf{F}^{(k)}}{\partial x} \right) dx dt \\ &= \int_{\mathcal{C}_i(t_0 + \Delta t)} \alpha^{(k)}(\mathbf{x}, t_0 + \Delta t) \mathbf{q}^{(k)}(\mathbf{x}, t_0 + \Delta t) d\mathbf{x} - \int_{\mathcal{C}_i(t_0)} \alpha^{(k)}(\mathbf{x}, t_0) \mathbf{q}^{(k)}(\mathbf{x}, t_0) d\mathbf{x} \\ &+ \int_{t_0}^{t_0 + \Delta t} \left( \alpha^{(k)}(x_{i+1/2}, t) \mathbf{F}^{(k)}(x_{i+1/2}, t) - \alpha^{(k)}(x_{i-1/2}, t) \mathbf{F}^{(k)}(x_{i-1/2}, t) \right) dt. \end{aligned} \quad (35)$$

Inserting (35) in (34), dividing by  $\Delta x$  and by  $\Delta t$  and taking the limit as  $\Delta t \rightarrow 0$  gives:

$$\frac{d}{dt} \left( \alpha_i^{(k)} \mathbf{q}_i^{(k)} \right) + \frac{1}{\Delta x} \left( \mathcal{E} \left( X \mathbf{F} \right)_{i+1/2}^{(k)} - \mathcal{E} \left( X \mathbf{F} \right)_{i-1/2}^{(k)} \right) = \frac{1}{\Delta x} \int_{\mathcal{C}_i} \mathcal{E} \left( \mathbf{S}^{(k)} \right) d\mathbf{x}. \quad (36)$$

The right-hand side of the above equation can be estimated by assuming a distribution of  $\mathbf{S}^{(k)}$  in the control volume  $\mathcal{C}_i$ . First, we assume that  $\mathbf{S}^{(k)}$  is constant in  $\mathcal{C}_i$ , to obtain a first-order approximation. The second-order scheme will be outlined in Section 3.3 on page 12.

The volume-fraction evolution equation (30) may also be integrated over  $\mathcal{C}_i \times [t_0, t_0 + \Delta t]$ :

$$\iint_{\mathcal{C}_i \times [t_0, t_0 + \Delta t]} \frac{\partial \alpha^{(k)}}{\partial t} dx dt = - \iint_{\mathcal{C}_i \times [t_0, t_0 + \Delta t]} \mathcal{E} \left( \mathbf{u}_{\text{int}}^{(k)} \cdot \nabla X^{(k)} \right) dx dt, \quad (37)$$

or

$$\begin{aligned} & \int_{\mathcal{C}_i(t_0 + \Delta t)} \alpha^{(k)}(\mathbf{x}, t_0 + \Delta t) d\mathbf{x} - \int_{\mathcal{C}_i(t_0)} \alpha^{(k)}(\mathbf{x}, t_0) d\mathbf{x} \\ &= - \iint_{\mathcal{C}_i \times [t_0, t_0 + \Delta t]} \mathcal{E} \left( \mathbf{u}_{\text{int}}^{(k)} \cdot \nabla X^{(k)} \right) dx dt. \end{aligned} \quad (38)$$

Divide by  $\Delta x$  and  $\Delta t$  and take the limit as  $\Delta t \rightarrow 0$ :

$$\frac{d\alpha_i^{(k)}}{dt} = - \int_{\mathcal{C}_i} \mathcal{E} \left( \mathbf{u}_{\text{int}}^{(k)} \cdot \nabla X^{(k)} \right) d\mathbf{x}. \quad (39)$$

This permits us to include the volume-fraction evolution equation into our system of equations, by writing

$$\frac{d}{dt} \left( \alpha_i^{(k)} \tilde{\mathbf{q}}_i^{(k)} \right) + \frac{1}{\Delta x} \left( \mathcal{E} \left( X \tilde{\mathbf{F}} \right)_{i+1/2}^{(k)} - \mathcal{E} \left( X \tilde{\mathbf{F}} \right)_{i-1/2}^{(k)} \right) = \frac{1}{\Delta x} \int_{\mathcal{C}_i} \mathcal{E} \left( \tilde{\mathbf{S}}^{(k)} \right) d\mathbf{x}, \quad (40)$$

where

$$\tilde{\mathbf{q}}^{(k)} = \left[ 1, \mathbf{q}^{(k)} \right]^T, \quad (41)$$

$$\tilde{\mathbf{F}}^{(k)} = \left[ 0, \mathbf{F}^{(k)} \right]^T, \quad (42)$$

and

$$\tilde{\mathbf{S}}^{(k)} = \left[ -\mathbf{u}_{\text{int}}^{(k)} \cdot \nabla X^{(k)}, \mathbf{S}^{(k)} \right]^T. \quad (43)$$

The discretization of the volume-fraction evolution equation is explained by Abgrall and Saurel [1]. Henceforth we use  $\tilde{\mathbf{q}}^{(k)}$ ,  $\tilde{\mathbf{F}}^{(k)}$ , and  $\tilde{\mathbf{S}}^{(k)}$ , but drop the tilde for convenience.

A main hypothesis in the Abgrall and Saurel [1] article is that it is reasonable to approximate the interface velocity  $\mathbf{u}_{\text{int}}^{(k)}(\xi_l)$  by the velocity of the contact discontinuity given by the Riemann problem between the states to the left and right of  $\xi_l$ . This is denoted by

$$\mathbf{S}^{(k)}(x) = \begin{cases} -\mathbf{F}^{\text{lag},(k)}(\mathbf{q}^{(k)}(x^-), \mathbf{q}^{(l)}(x^+)) & \text{if } [X^{(k)}] = -1, \\ \mathbf{F}^{\text{lag},(k)}(\mathbf{q}^{(l)}(x^-), \mathbf{q}^{(k)}(x^+)) & \text{if } [X^{(k)}] = 1, \end{cases} \quad (44)$$

where  $k$  is the phase under consideration and  $l$  is the other phase.  $x^-$  is the coordinate to the left of  $x$  and  $x^+$  is to the right. The jump in  $X^{(k)}$  at  $x$ ,  $[X^{(k)}] = X^{(k),+} - X^{(k),-} = \pm 1$  is negative when we have phase  $k$  to the left and phase  $l$  to the right, since then,  $X^{(k)} = 0$  to the left and  $X^{(k)} = 1$  to the right.

To estimate the right-hand side of (36), we must consider the boundaries and the interior of the control volume  $\mathcal{C}_i$  separately. At the boundary  $x_{i-1/2}$ , the discontinuity will only count if the interfacial velocity is positive, else it will be counted in the control volume to the left. Conversely, at the boundary  $x_{i+1/2}$  the discontinuity will only count if the interfacial velocity is negative.

It is also necessary to consider the probability of having phase  $k$  to the left of  $x_{i+1/2}$  and phase  $l$  to the right, etc. These probabilities are denoted by  $\mathcal{P}_{i+1/2}(k, l)$ , and, as explained by Abgrall and Saurel [1], reasonable estimates are

$$\begin{aligned} \mathcal{P}_{i+1/2}(k, k) &= \min(\alpha_i^{(k)}, \alpha_{i+1}^{(k)}), \\ \mathcal{P}_{i+1/2}(k, l) &= \max(\alpha_i^{(k)} - \alpha_{i+1}^{(k)}, 0), \end{aligned} \quad (45)$$

Using all this, we get for the boundary part of the right-hand side of (36):

$$\begin{aligned}
\int_{\mathcal{C}_i} \mathcal{E}(\mathbf{S}^{(k)})_{\text{bound}} dx &= \int_{\mathcal{C}_i} \mathcal{E} \left( \mathbf{F}^{\text{lag},(k)} \frac{\partial X^{(k)}}{\partial x} \right)_{\text{bound}} dx \\
&= -\max\left\{0, \text{sgn}[\mathbf{u}_{\text{int}}^{(k)}(\mathbf{q}_{i-1/2}^{(k,-)}, \mathbf{q}_{i-1/2}^{(l,+)})]\right\} \mathcal{P}_{i-1/2}(k, l) \mathbf{F}^{\text{lag},(k)}(\mathbf{q}_{i-1/2}^{(k,-)}, \mathbf{q}_{i-1/2}^{(l,+)}) \\
&\quad + \max\left\{0, \text{sgn}[\mathbf{u}_{\text{int}}^{(k)}(\mathbf{q}_{i-1/2}^{(l,-)}, \mathbf{q}_{i-1/2}^{(k,+)})]\right\} \mathcal{P}_{i-1/2}(l, k) \mathbf{F}^{\text{lag},(k)}(\mathbf{q}_{i-1/2}^{(l,-)}, \mathbf{q}_{i-1/2}^{(k,+)}) \\
&\quad + \min\left\{0, \text{sgn}[\mathbf{u}_{\text{int}}^{(k)}(\mathbf{q}_{i+1/2}^{(k,-)}, \mathbf{q}_{i+1/2}^{(l,+)})]\right\} \mathcal{P}_{i+1/2}(k, l) \mathbf{F}^{\text{lag},(k)}(\mathbf{q}_{i+1/2}^{(k,-)}, \mathbf{q}_{i+1/2}^{(l,+)}) \\
&\quad - \min\left\{0, \text{sgn}[\mathbf{u}_{\text{int}}^{(k)}(\mathbf{q}_{i+1/2}^{(l,-)}, \mathbf{q}_{i+1/2}^{(k,+)})]\right\} \mathcal{P}_{i+1/2}(l, k) \mathbf{F}^{\text{lag},(k)}(\mathbf{q}_{i+1/2}^{(l,-)}, \mathbf{q}_{i+1/2}^{(k,+)}) .
\end{aligned} \tag{46}$$

The part of the right-hand side of (36) arising from internal interfaces, is called relaxation terms by Abgrall and Saurel [1]. Denote the expected number of internal interfaces by  $N_{\text{int},i}$ . Similarly to what was done above, and using the midpoint rule, this gives:

$$\begin{aligned}
\int_{\mathcal{C}_i} \mathcal{E}(\mathbf{S}^{(k)})_{\text{relax}} dx &= \int_{\mathcal{C}_i} \mathcal{E} \left( \mathbf{F}^{\text{lag},(k)} \frac{\partial X^{(k)}}{\partial x} \right)_{\text{relax}} dx \\
&= \frac{N_{\text{int},i}}{2} \left( \mathbf{F}^{\text{lag},(k)}(\mathbf{q}_i^{(l)}, \mathbf{q}_i^{(k)}) - \mathbf{F}^{\text{lag},(k)}(\mathbf{q}_i^{(k)}, \mathbf{q}_i^{(l)}) \right), \tag{47}
\end{aligned}$$

where the second equality depends on the assumption that  $\mathbf{F}^{\text{lag},(k)} \partial X^{(k)} / \partial x$  is constant in  $\mathcal{C}_i$ . Hence,

$$\int_{\mathcal{C}_i} \mathcal{E}(\mathbf{S}^{(k)}) dx = \int_{\mathcal{C}_i} \mathcal{E}(\mathbf{S}^{(k)})_{\text{bound}} dx + \int_{\mathcal{C}_i} \mathcal{E}(\mathbf{S}^{(k)})_{\text{relax}} dx, \tag{48}$$

using (46) and (47).

### 3.2 Conservative fluxes

Now consider the flux terms on the right-hand side of (36). For the control-volume boundary at  $x_{i+1/2}$ , we have, of course, a contribution to the phase  $k$ -equation if there is phase  $k$  on both sides. Moreover, there is a contribution if phase  $k$  exists on the left-hand side and phase  $l$  on the right-hand side, if the interface velocity is positive (phase  $k$  exits), and finally there is a contribution if phase  $l$  exists on the left-hand side and  $k$  on the right-hand side, if the interface velocity is negative (phase  $k$  enters). If we have phase  $l$  on both sides, there is no contribution to the phase  $k$ -equation.

Hence,

$$\begin{aligned}
\mathcal{E}(XF)_{i+1/2}^{(k)} &= \mathcal{P}_{i+1/2}(k, k) \mathbf{F}^{(k)}(\mathbf{q}_i^{(k)}, \mathbf{q}_{i+1}^{(k)}) \\
&\quad + \max\left\{0, \operatorname{sgn}[\mathbf{u}_{\text{int}}^{(k)}(\mathbf{q}_i^{(k)}, \mathbf{q}_{i+1}^{(l)})]\right\} \mathcal{P}_{i+1/2}(k, l) \mathbf{F}^{(k)}(\mathbf{q}_i^{(k)}, \mathbf{q}_{i+1}^{(l)}) \\
&\quad + \max\left\{0, \operatorname{sgn}[-\mathbf{u}_{\text{int}}^{(k)}(\mathbf{q}_i^{(l)}, \mathbf{q}_{i+1}^{(k)})]\right\} \mathcal{P}_{i+1/2}(l, k) \mathbf{F}^{(k)}(\mathbf{q}_i^{(l)}, \mathbf{q}_{i+1}^{(k)}).
\end{aligned} \tag{49}$$

At the control-volume boundary at  $x_{i-1/2}$  the situation is similar.

### 3.3 Second-order scheme

With (46)–(49), we can advance (36) in time using an appropriate scheme. Abgrall and Saurel [1] proposed to use a modified MUSCL-Hancock scheme [18] [see 17, Section 14.4] to get second-order accuracy in space and time. This will not be repeated here, except that one point will be made: Extra terms arise in  $\mathcal{E}(\mathbf{S}^{(k)})_{\text{bound}}$  for the second-order scheme. This is due to the fact that for a first-order Godunov method, the variables are assumed to be constant in each control volume  $\mathcal{C}_i$ , whereas in the second-order method, they are assumed to be linearly varying.

To see how the extra terms arise, divide the cell  $\mathcal{C}_i$  into  $M + 1$  sub-cells ( $x_{i-1/2} = \eta_{0-1/2}, \dots, \eta_{j-1/2}, \dots, \eta_{M+1/2} = x_{i+1/2}$ ;  $j \in \{0, 1, \dots, M + 1\}$ ;  $\Delta\eta = \eta_{j+1/2} - \eta_{j-1/2} = \Delta x / (M + 1)$ ) in which the volume fraction  $\alpha_j^{(k)}$  is supposed to be constant. Both fluids can exist in each of these  $M + 1$  sub-cells. Then divide each of the sub-cells into  $N$  sub-sub-cells containing pure phase  $k$  or  $l$ . Hence the first-order scheme previously found can be directly applied to each of the  $M + 1$  sub-cells. However, since the volume fraction  $\alpha_j^{(k)}$  is supposed to be constant for each  $j$ , it is necessary to let  $M \rightarrow \infty$  to obtain the assumed linear distribution.

Apply the semi-discrete scheme to the  $M + 1$  sub-cells:

$$\begin{aligned}
\frac{d}{dt}(\alpha_j^{(k)} \mathbf{q}_j^{(k)}) &+ \frac{1}{\Delta\eta} \left( \mathcal{E}(XF)_{j+1/2}^{(k)} - \mathcal{E}(XF)_{j-1/2}^{(k)} \right) \\
&= \frac{1}{\Delta\eta} \int_{x \in [\eta_{j-1/2}, \eta_{j+1/2}]} \left\{ \mathcal{E}(\mathbf{S}^{(k)})_{\text{bound}} + \mathcal{E}(\mathbf{S}^{(k)})_{\text{relax}} \right\} dx. \tag{50}
\end{aligned}$$

To obtain an equation for the cell  $\mathcal{C}_i$ , multiply the above equation with

$\Delta\eta$  and sum it term-wise. The first term becomes

$$\begin{aligned} \sum_{j=0}^M \Delta\eta \frac{d}{dt} (\alpha_j^{(k)} \mathbf{q}_j^{(k)}) &= \sum_{j=0}^M \frac{\Delta x}{M+1} \frac{d}{dt} (\alpha_j^{(k)} \mathbf{q}_j^{(k)}) \\ &= \Delta x \frac{d}{dt} \left( \frac{1}{M+1} \sum_{j=0}^M \alpha_j^{(k)} \mathbf{q}_j^{(k)} \right), \end{aligned} \quad (51)$$

that is, we calculate the mean of the conserved variables. The Eulerian fluxes are evaluated in the following way:

$$\sum_{j=0}^M \left( \mathcal{E}(\mathbf{XF})_{j+1/2}^{(k)} - \mathcal{E}(\mathbf{XF})_{j-1/2}^{(k)} \right) = \mathcal{E}(\mathbf{XF})_{M+1/2}^{(k)} - \mathcal{E}(\mathbf{XF})_{1/2}^{(k)}, \quad (52)$$

that is, the sum telescopes. The right-hand side becomes

$$\sum_{j=0}^M \int_{x \in [\eta_{j-1/2}, \eta_{j+1/2}]} \left\{ \mathcal{E}(\mathbf{S}^{(k)})_{\text{bound}} + \mathcal{E}(\mathbf{S}^{(k)})_{\text{relax}} \right\} dx, \quad (53)$$

where

$$\begin{aligned} \int_{x \in [\eta_{j-1/2}, \eta_{j+1/2}]} \left\{ \mathcal{E}(\mathbf{S}^{(k)})_{\text{bound}} + \mathcal{E}(\mathbf{S}^{(k)})_{\text{relax}} \right\} dx &= \\ &- \max \left\{ 0, \text{sgn}[\mathbf{u}_{\text{int}}^{(k)}(\mathbf{q}_{j-1}^{(k)}, \mathbf{q}_j^{(l)})] \right\} \mathcal{P}_{j-1/2}(k, l) \mathbf{F}^{\text{lag},(k)}(\mathbf{q}_{j-1}^{(k)}, \mathbf{q}_j^{(l)}) \\ &+ \max \left\{ 0, \text{sgn}[\mathbf{u}_{\text{int}}^{(k)}(\mathbf{q}_{j-1}^{(l)}, \mathbf{q}_j^{(k)})] \right\} \mathcal{P}_{j-1/2}(l, k) \mathbf{F}^{\text{lag},(k)}(\mathbf{q}_{j-1}^{(l)}, \mathbf{q}_j^{(k)}) \\ &+ \min \left\{ 0, \text{sgn}[\mathbf{u}_{\text{int}}^{(k)}(\mathbf{q}_j^{(k)}, \mathbf{q}_{j+1}^{(l)})] \right\} \mathcal{P}_{j+1/2}(k, l) \mathbf{F}^{\text{lag},(k)}(\mathbf{q}_j^{(k)}, \mathbf{q}_{j+1}^{(l)}) \\ &- \min \left\{ 0, \text{sgn}[\mathbf{u}_{\text{int}}^{(k)}(\mathbf{q}_j^{(l)}, \mathbf{q}_{j+1}^{(k)})] \right\} \mathcal{P}_{j+1/2}(l, k) \mathbf{F}^{\text{lag},(k)}(\mathbf{q}_j^{(l)}, \mathbf{q}_{j+1}^{(k)}) \\ &+ \frac{N_{\text{int},j}}{2} \left( \mathbf{F}^{\text{lag},(k)}(\mathbf{q}_j^{(l)}, \mathbf{q}_j^{(k)}) - \mathbf{F}^{\text{lag},(k)}(\mathbf{q}_j^{(k)}, \mathbf{q}_j^{(l)}) \right). \end{aligned} \quad (54)$$

First consider the terms of the type  $\mathbf{F}^{\text{lag},(k)}(\mathbf{q}_m^{(k)}, \mathbf{q}_{m+1}^{(l)})$ , that is,

$$\begin{aligned} &\sum_{j=0}^M \left\{ \min \left\{ 0, \text{sgn}[\mathbf{u}_{\text{int}}^{(k)}(\mathbf{q}_j^{(k)}, \mathbf{q}_{j+1}^{(l)})] \right\} \mathcal{P}_{j+1/2}(k, l) \mathbf{F}^{\text{lag},(k)}(\mathbf{q}_j^{(k)}, \mathbf{q}_{j+1}^{(l)}) \right. \\ &\quad \left. - \max \left\{ 0, \text{sgn}[\mathbf{u}_{\text{int}}^{(k)}(\mathbf{q}_{j-1}^{(k)}, \mathbf{q}_j^{(l)})] \right\} \mathcal{P}_{j-1/2}(k, l) \mathbf{F}^{\text{lag},(k)}(\mathbf{q}_{j-1}^{(k)}, \mathbf{q}_j^{(l)}) \right\} \\ &= \sum_{j=0}^M \left\{ \min \left\{ 0, \text{sgn}[\mathbf{u}_{\text{int}}^{(k)}(\mathbf{q}_j^{(k)}, \mathbf{q}_{j+1}^{(l)})] \right\} \max(\alpha_j^{(k)} - \alpha_{j+1}^{(k)}, 0) \mathbf{F}^{\text{lag},(k)}(\mathbf{q}_j^{(k)}, \mathbf{q}_{j+1}^{(l)}) \right. \\ &\quad \left. - \max \left\{ 0, \text{sgn}[\mathbf{u}_{\text{int}}^{(k)}(\mathbf{q}_{j-1}^{(k)}, \mathbf{q}_j^{(l)})] \right\} \max(\alpha_{j-1}^{(k)} - \alpha_j^{(k)}, 0) \mathbf{F}^{\text{lag},(k)}(\mathbf{q}_{j-1}^{(k)}, \mathbf{q}_j^{(l)}) \right\}. \end{aligned} \quad (55)$$

Define

$$V_m = \max(\alpha_m^{(k)} - \alpha_{m+1}^{(k)}, 0) \mathbf{F}^{\text{lag},(k)}(\mathbf{q}_m^{(k)}, \mathbf{q}_{m+1}^{(l)}), \quad (56)$$

$$\left(\beta_{m-1/2}^{(k,l)}\right)^+ = \max\{0, \text{sgn}[\mathbf{u}_{\text{int}}^{(k)}(\mathbf{q}_{m-1}^{(k)}, \mathbf{q}_m^{(l)})]\}, \quad (57)$$

and

$$\left(\beta_{m+1/2}^{(k,l)}\right)^- = \min\{0, \text{sgn}[\mathbf{u}_{\text{int}}^{(k)}(\mathbf{q}_m^{(k)}, \mathbf{q}_{m+1}^{(l)})]\}, \quad (58)$$

so that the sum in (55) can be written as

$$\begin{aligned} \sum_{j=0}^M \left\{ \left(\beta_{j+1/2}^{(k,l)}\right)^- V_j - \left(\beta_{j-1/2}^{(k,l)}\right)^+ V_{j-1} \right\} &= \sum_{j=0}^M \left(\beta_{j+1/2}^{(k,l)}\right)^- V_j - \sum_{j=-1}^{M-1} \left(\beta_{j+1/2}^{(k,l)}\right)^+ V_j \\ &= \left(\beta_{M+1/2}^{(k,l)}\right)^- V_M - \left(\beta_{-1/2}^{(k,l)}\right)^+ V_0 - \sum_{j=0}^{M-1} V_j. \end{aligned} \quad (59)$$

The two first terms on the right-hand side above correspond to the interactions with the cells  $\mathcal{C}_{i+1}$  and  $\mathcal{C}_{i-1}$ , respectively. The last term is

$$\begin{aligned} \sum_{j=0}^{M-1} V_j &= \sum_{j=0}^{M-1} \max(\alpha_j^{(k)} - \alpha_{j+1}^{(k)}, 0) \mathbf{F}^{\text{lag},(k)}(\mathbf{q}_j^{(k)}, \mathbf{q}_{j+1}^{(l)}) \\ &= \sum_{j=0}^{M-1} (\eta_{j+1} - \eta_j) \max(-\delta_i \alpha_i^{(k)}, 0) \mathbf{F}^{\text{lag},(k)}(\mathbf{q}_j^{(k)}, \mathbf{q}_{j+1}^{(l)}) \\ &= \max(-\delta_i \alpha_i^{(k)}, 0) \sum_{j=0}^{M-1} (\eta_{j+1} - \eta_j) \mathbf{F}^{\text{lag},(k)}(\mathbf{q}_j^{(k)}, \mathbf{q}_{j+1}^{(l)}) \\ &= \max(\delta_i \alpha_i^{(l)}, 0) \sum_{j=0}^{M-1} (\eta_{j+1} - \eta_j) \mathbf{F}^{\text{lag},(k)}(\mathbf{q}_j^{(k)}, \mathbf{q}_{j+1}^{(l)}), \end{aligned} \quad (60)$$

where  $\delta_i \alpha_i^{(k)}$  is the slope of the volume fraction in the  $i$ th cell, given by the chosen limiter function. The last sum is a Riemann sum, and therefore

$$\lim_{M \rightarrow \infty} \sum_{j=0}^{M-1} V_j = \max(\delta_i \alpha_i^{(l)}, 0) \int_{x_{i-1/2}}^{x_{i+1/2}} \mathbf{F}^{\text{lag},(k)}(\mathbf{q}^{(k)}(\eta), \mathbf{q}^{(l)}(\eta)) d\eta. \quad (61)$$

The above integral can be estimated using the second-order midpoint method:

$$\int_{x_{i-1/2}}^{x_{i+1/2}} \mathbf{F}^{\text{lag},(k)}(\mathbf{q}^{(k)}(\eta), \mathbf{q}^{(l)}(\eta)) d\eta \approx \mathbf{F}^{\text{lag},(k)}(\mathbf{q}_i^{(k)}, \mathbf{q}_i^{(l)}) \Delta x. \quad (62)$$

Here,  $\mathbf{q}_i^{(k)}$  is evaluated at  $(x_{i+1/2} - x_{i-1/2})/2 = x_i$ .

Using exactly the same arguments, but reversing the phasic indices  $k$  and  $l$ , we arrive at the corresponding expression for  $\mathbf{F}^{\text{lag},(k)}(\mathbf{q}_m^{(l)}, \mathbf{q}_{m+1}^{(k)})$ ,

namely,

$$\begin{aligned}
& \sum_{j=0}^M \left\{ \max \left\{ 0, \operatorname{sgn}[\mathbf{u}_{\text{int}}^{(k)}(\mathbf{q}_{j-1}^{(l)}, \mathbf{q}_j^{(k)})] \right\} \mathcal{P}_{j-1/2}(l, k) \mathbf{F}^{\text{lag},(k)}(\mathbf{q}_{j-1}^{(l)}, \mathbf{q}_j^{(k)}) \right. \\
& \quad \left. - \min \left\{ 0, \operatorname{sgn}[\mathbf{u}_{\text{int}}^{(k)}(\mathbf{q}_j^{(l)}, \mathbf{q}_{j+1}^{(k)})] \right\} \mathcal{P}_{j+1/2}(l, k) \mathbf{F}^{\text{lag},(k)}(\mathbf{q}_j^{(l)}, \mathbf{q}_{j+1}^{(k)}) \right\} \\
& \quad \approx \max(\delta_i \alpha_i^{(k)}, 0) \mathbf{F}^{\text{lag},(k)}(\mathbf{q}_i^{(l)}, \mathbf{q}_i^{(k)}) \Delta x + \text{boundary terms.} \quad (63)
\end{aligned}$$

For the relaxation terms, we obtain analogously, using the midpoint rule:

$$\begin{aligned}
& \sum_{j=0}^M \left\{ \frac{N_{\text{int},j}}{2} \left( \mathbf{F}^{\text{lag},(k)}(\mathbf{q}_j^{(l)}, \mathbf{q}_j^{(k)}) - \mathbf{F}^{\text{lag},(k)}(\mathbf{q}_j^{(k)}, \mathbf{q}_j^{(l)}) \right) \right\} \\
& \quad \approx \frac{N_{\text{int},i}}{2} \left( \mathbf{F}^{\text{lag},(k)}(\mathbf{q}_i^{(l)}, \mathbf{q}_i^{(k)}) - \mathbf{F}^{\text{lag},(k)}(\mathbf{q}_i^{(k)}, \mathbf{q}_i^{(l)}) \right), \quad (64)
\end{aligned}$$

so that the final, second-order expression for phase-interaction terms becomes:

$$\begin{aligned}
& \sum_{j=0}^M \int_{x \in [\eta_{j-1/2}, \eta_{j+1/2}]} \left\{ \mathcal{E}(\mathbf{s}^{(k)})_{\text{bound}} + \mathcal{E}(\mathbf{s}^{(k)})_{\text{relax}} \right\} dx \approx \\
& \quad \text{I} \left\{ \begin{aligned}
& - \max \left\{ 0, \operatorname{sgn}[\mathbf{u}_{\text{int}}^{(k)}(\mathbf{q}_{i-1/2}^{(k,-)}, \mathbf{q}_{i-1/2}^{(l,+)})] \right\} \mathcal{P}_{i-1/2}(k, l) \mathbf{F}^{\text{lag},(k)}(\mathbf{q}_{i-1/2}^{(k,-)}, \mathbf{q}_{i-1/2}^{(l,+)}) \\
& + \max \left\{ 0, \operatorname{sgn}[\mathbf{u}_{\text{int}}^{(k)}(\mathbf{q}_{i-1/2}^{(l,-)}, \mathbf{q}_{i-1/2}^{(k,+)})] \right\} \mathcal{P}_{i-1/2}(l, k) \mathbf{F}^{\text{lag},(k)}(\mathbf{q}_{i-1/2}^{(l,-)}, \mathbf{q}_{i-1/2}^{(k,+)}) \\
& + \min \left\{ 0, \operatorname{sgn}[\mathbf{u}_{\text{int}}^{(k)}(\mathbf{q}_{i+1/2}^{(k,-)}, \mathbf{q}_{i+1/2}^{(l,+)})] \right\} \mathcal{P}_{i+1/2}(k, l) \mathbf{F}^{\text{lag},(k)}(\mathbf{q}_{i+1/2}^{(k,-)}, \mathbf{q}_{i+1/2}^{(l,+)}) \\
& - \min \left\{ 0, \operatorname{sgn}[\mathbf{u}_{\text{int}}^{(k)}(\mathbf{q}_{i+1/2}^{(l,-)}, \mathbf{q}_{i+1/2}^{(k,+)})] \right\} \mathcal{P}_{i+1/2}(l, k) \mathbf{F}^{\text{lag},(k)}(\mathbf{q}_{i+1/2}^{(l,-)}, \mathbf{q}_{i+1/2}^{(k,+)}) \\
& + \frac{N_{\text{int},i}}{2} \left( \mathbf{F}^{\text{lag},(k)}(\mathbf{q}_i^{(l)}, \mathbf{q}_i^{(k)}) - \mathbf{F}^{\text{lag},(k)}(\mathbf{q}_i^{(k)}, \mathbf{q}_i^{(l)}) \right)
\end{aligned} \right. \\
& \quad \text{II} \left\{ \begin{aligned}
& - \max(\delta_i \alpha_i^{(l)}, 0) \mathbf{F}^{\text{lag},(k)}(\mathbf{q}_i^{(k)}, \mathbf{q}_i^{(l)}) \Delta x \\
& + \max(\delta_i \alpha_i^{(k)}, 0) \mathbf{F}^{\text{lag},(k)}(\mathbf{q}_i^{(l)}, \mathbf{q}_i^{(k)}) \Delta x.
\end{aligned} \right. \quad (65)
\end{aligned}$$

Herein, (I) represent the MUSCL method and relaxation terms, and (II) are correction terms. Note that they involve Riemann problems between the two phases, centred in the computational cells and not at the cell interfaces. As shown above, they arise from the non-conservative terms,  $\mathbf{F}^{\text{lag},(k)}$ , in (I). Further details are discussed by Papin [13, Part II, Chapter 3].

### 3.4 Comparison with ‘conventional’ model

The ‘conventional’, continuous model given by (1) and (2) can be written as

$$\frac{\partial \alpha^{(k)} \hat{\mathbf{q}}^{(k)}}{\partial t} + \nabla \cdot (\alpha^k \hat{\mathbf{F}}^{(k)}) = \hat{\mathbf{S}}^{(k)}, \quad (66)$$

where

$$\hat{\mathbf{q}}^{(k)} = \left[ \rho^{(k)}, \rho^{(k)} \mathbf{u}^{(k)} \right]^T, \quad (67)$$

$$\hat{\mathbf{F}}^{(k)} = \left[ \rho^{(k)} \mathbf{u}^{(k)}, \rho^{(k)} (\mathbf{u}^{(k)})^2 + \mathbf{p}^{(k)} \right]^T, \quad (68)$$

and

$$\hat{\mathbf{S}}^{(k)} = \left[ 0, \mathbf{p}_{\text{int}}^{(k)} \frac{\partial \alpha^{(k)}}{\partial \mathbf{x}} \right]^T. \quad (69)$$

Recall the present (semi-) discrete model (40):

$$\begin{aligned} \frac{d}{dt} (\alpha_i^{(k)} \mathbf{q}_i^{(k)}) + \frac{1}{\Delta \mathbf{x}} \left( \mathcal{E} (X\mathbf{F})_{i+1/2}^{(k)} - \mathcal{E} (X\mathbf{F})_{i-1/2}^{(k)} \right) \\ = \frac{1}{\Delta \mathbf{x}} \int_{\mathcal{E}_i} \left\{ \mathcal{E} (\mathbf{S}^{(k)})_{\text{bound}} + \mathcal{E} (\mathbf{S}^{(k)})_{\text{relax}} \right\} d\mathbf{x}, \end{aligned} \quad (70)$$

where

$$\mathbf{q}^{(k)} = \left[ 1, \rho^{(k)}, \rho^{(k)} \mathbf{u}^{(k)} \right]^T, \quad (71)$$

$$\mathbf{F}^{(k)} = \left[ 0, \rho^{(k)} \mathbf{u}^{(k)}, \rho^{(k)} (\mathbf{u}^{(k)})^2 + \mathbf{p}^{(k)} \right]^T, \quad (72)$$

and

$$\mathbf{S}^{(k)} = \left[ -\mathbf{u}_{\text{int}}^{(k)} \frac{\partial X^{(k)}}{\partial \mathbf{x}}, 0, \mathbf{p}^{(k)} \frac{\partial X^{(k)}}{\partial \mathbf{x}} \right]^T. \quad (73)$$

The system (70) has one more equation than (66); it is the volume-fraction equation. Hence, (70) has a priori two independent pressures, while (66) has only one (See Section 3.6 on page 20). In the ‘conventional’ model, the volume fraction can be found using the equation of state (22), the pressure equality, and the relation  $\alpha_g + \alpha_\ell = 1$ , whereas in the discrete-equation model, the volume fraction is found from a transport equation.

Except for the above-mentioned differences, the left-hand sides are analogous.  $\hat{\mathbf{q}}^{(k)}$  is (implicitly) volume-averaged, while  $\mathbf{q}^{(k)}$  is ensemble-averaged.  $\hat{\mathbf{F}}^{(k)}$  is implicitly volume-averaged, while the ensemble-averaging of  $\mathbf{F}^{(k)}$  is shown explicitly.

The correspondence between the right-hand sides is more subtle. The right-hand side of (70) can be substituted by the right-hand side of (65). The expression  $\hat{\mathbf{S}}^{(k)}$  for the ‘conventional’ model is simpler, but a lot of

necessary modelling effort is hidden away in the interfacial pressure  $p_{\text{int}}^{(k)}$ . Several of the interfacial-pressure models presented in the literature seem to be chosen such that the eigenvalues of the resulting system coefficient matrix are real for a range of suitable flow conditions. One of the main advantages of the present method, on the other hand, is that it avoids several problems regarding hyperbolicity. This is discussed somewhat further in Section 3.7.

Note that the pressure  $p^{(k)}$  in (73) is the pressure at the interface, hence there is a connection to the ‘conventional’ model (69). However, in the discrete model, the interfacial pressure and velocity come from the solution of Riemann problems at the interface. We hypothesize that this might be a useful point of view with respect to the modelling of the interfacial quantities.

### 3.5 *The Riemann problem*

Due to the discrete nature of the present model, the Riemann problems to be solved are between two pure fluids. Hence, the equations defining the Riemann problems are the isentropic Euler equations with the addition of an advection equation for the phase-indicator function. The employed equation of state may have different parameters in the two states.

The solution to the Riemann problem for fluid dynamics is described by Toro [17], LeVeque [10]. However, LeVeque [9] gives details with respect to the isentropic Euler equations.

For the isentropic Euler equations, there is no contact discontinuity, therefore one cannot distinguish between the fluids on the right-hand and on the left-hand sides. However, in the present case there is also an advection equation for the phase-indicator function, which adds the required contact discontinuity. Hence the hypothesis of Abgrall and Saurel [1] that the volume fraction is advected by the speed given by the corresponding Riemann problem, often denoted by  $u^*$ , see Figure 2 on the next page. On each side of the point moving with speed  $u^*$ , we have pure phase  $k$  or  $l$ . Moreover, the Rankine-Hugoniot relations imply that at this point, there must be equality of pressure (denoted by  $p^*$ ) between the left-hand and right-hand states. Therefore, the Riemann problem can be solved.

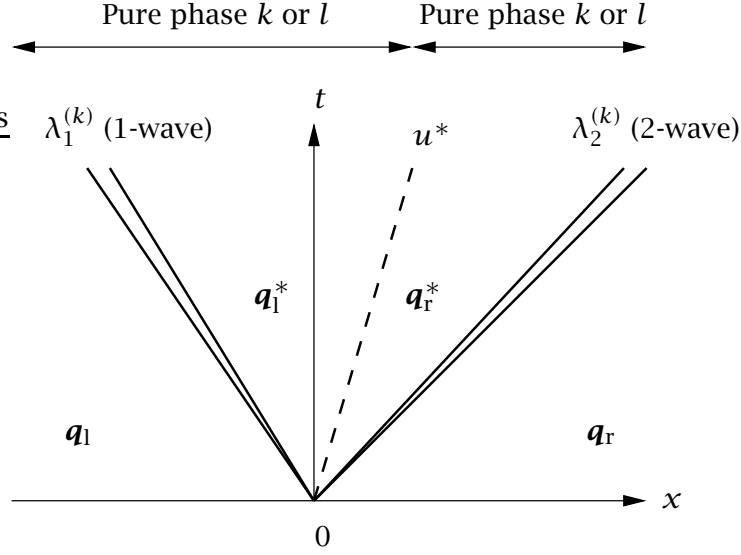


Figure 2. Structure of the solution to the Riemann problem.

The equations defining the Riemann problem are

$$\begin{aligned}
\frac{\partial X^{(k)}}{\partial t} + u_{\text{int}}^{(k)} \frac{\partial X^{(k)}}{\partial x} &= 0, \\
\frac{\partial}{\partial t} (X^{(k)} \rho^{(k)}) + \frac{\partial}{\partial x} (X^{(k)} \rho^{(k)} u^{(k)}) &= 0, \\
\frac{\partial}{\partial t} (X^{(l)} \rho^{(l)}) + \frac{\partial}{\partial x} (X^{(l)} \rho^{(l)} u^{(l)}) &= 0, \\
\frac{\partial}{\partial t} (X^{(k)} \rho^{(k)} u^{(k)}) + \frac{\partial}{\partial x} (X^{(k)} \rho^{(k)} u^{(k)} u^{(k)} + X^{(k)} p^{(k)}) &= 0, \\
\frac{\partial}{\partial t} (X^{(l)} \rho^{(l)} u^{(l)}) + \frac{\partial}{\partial x} (X^{(l)} \rho^{(l)} u^{(l)} u^{(l)} + X^{(l)} p^{(l)}) &= 0,
\end{aligned} \tag{74}$$

where we take  $u_{\text{int}}^{(k)} = u^*$ . Since either  $X^{(k)}$  or  $X^{(l)}$  is zero on each side of the contact discontinuity, it suffices to solve the Riemann problem corresponding to the pure-phase isentropic Euler equations, using the appropriate equation of state.

Another way to look at (74), is to write

$$\begin{aligned}
\frac{\partial X^{(k)}}{\partial t} + u_{\text{int}} \frac{\partial X}{\partial x} &= 0, \\
\frac{\partial}{\partial t} (\rho) + \frac{\partial}{\partial x} (\rho u) &= 0, \\
\frac{\partial}{\partial t} (\rho u) + \frac{\partial}{\partial x} (\rho u u + p) &= 0,
\end{aligned} \tag{75}$$

where the equation of state is  $p = p(\rho, X^{(k)})$ , that is, the equation of state of phase  $k$  is employed when  $X^{(k)} = 1$  and the equation of state of phase  $l$  is used otherwise. The velocity  $u$  is constant across the con-

tact discontinuity, that is,  $u_1^* = u_r^*$ . Moreover  $u = u_{\text{int}}$  there. Hence the Rankine-Hugoniot conditions

$$\begin{aligned} [\rho(u - u_{\text{int}})] &= 0, \\ [\rho u(u - u_{\text{int}}) + p] &= 0, \end{aligned} \quad (76)$$

imply that  $p_1^* = p_r^*$ .

The velocity as a function of pressure through a rarefaction wave is given by

$$u^{(k)}(p^{(k)}) = u_s^{(k)} \pm c^{(k)} \ln \left\{ \frac{p^{(k)} + \rho_o^{(k)}(c^{(k)})^2}{p_s^{(k)} + \rho_o^{(k)}(c^{(k)})^2} \right\}, \quad (77)$$

where the negative sign corresponds to the eigenvalue  $\lambda_1^{(k)} = u^{(k)} - c^{(k)}$  and the positive sign corresponds to  $\lambda_2^{(k)} = u^{(k)} + c^{(k)}$ . The subscript  $s$  denotes the known state, that is, the left state for  $\lambda_1^{(k)}$  and the right state for  $\lambda_2^{(k)}$ .

Across a shock, the velocity function is

$$u^{(k)}(p^{(k)}) = u_s^{(k)} \pm \frac{p^{(k)} - p_s^{(k)}}{c^{(k)} \sqrt{(p^{(k)} + \rho_o^{(k)}(c^{(k)})^2)(p_s^{(k)} + \rho_o^{(k)}(c^{(k)})^2)}}, \quad (78)$$

when the equation of state (22) is used, where again the negative sign corresponds to the eigenvalue  $\lambda_1^{(k)} = u^{(k)} - c^{(k)}$  and the positive sign corresponds to  $\lambda_2^{(k)} = u^{(k)} + c^{(k)}$ . If  $p^* > p_l$ , then the 1-wave is a shock, else it is a rarefaction. Similarly, if  $p^* > p_r$ , then the 2-wave is a shock, else it is a rarefaction. Using this, equations (77) and (78), as well as the procedure described by Toro [17, Section 4.5], an exact Riemann solver has been written. However, for the presently-considered test problems, an acoustic solver, or ‘primitive-variables Riemann solver’ (PVRS), [17, Section 9.3] gave very similar results, and shorter (in the order of 50%) CPU times.

The principle of the acoustic solver is a linearization of the shock and rarefaction waves. In the present work, we have chosen to use the acoustic solver for two reasons: Simplicity and robustness. The robustness is required since we solve Riemann problems between two pure fluids with possibly very different equation-of-state parameters. Other possible choices for approximate Riemann solvers are HLL-type schemes, relaxation schemes, etc.

Consider the solution to the liquid–gas Riemann problem shown in Figure 3(a) on the following page. The left-hand state is gas, whereas the right-hand state is liquid. The input data correspond to the ‘Shock tube 2’ test case, described in Section 5.2 on page 27. The curves in the figure are plots of (77). The legend ‘q11’ denotes the curve corresponding to  $\lambda_1$

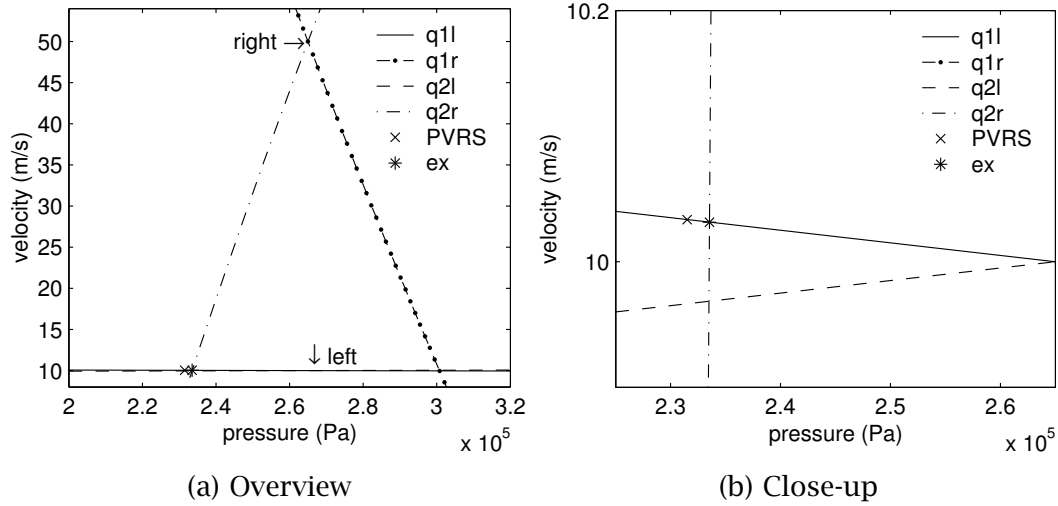


Figure 3. Solution to a liquid-gas Riemann problem.

going through the left-hand state. Analogously, ‘q2r’ is for  $\lambda_2$  and goes through the right-hand state, etc. The curves for the liquid have a much smaller gradient than those for the gas, since the liquid has a higher speed of sound. The exact solution to the Riemann problem, denoted by ‘ex’ in the figure, lies, in this case, on the intersection between the 1-rarefaction from the left and the 2-rarefaction from the right. As can be observed in Figure 3(b), the solution given by the acoustic solver (‘PVRS’) was not much off; the predicted velocity was 0.02% too high and the pressure was 0.9% too low. The curves plotted using (77) and (78) were very nearly linear and hardly distinguishable.

More physical phenomena, for instance surface tension, can be accounted for in the discrete-equation model by including them in the Riemann-problem definition. This, as well as viscous flows and other equations of state, is discussed in more detail by Papin [13]. It is also possible to treat phase transition [8].

### 3.6 Pressure relaxation

For the two-phase flows considered here, neglecting surface tension and other effects, it is reasonable to assume pressure equality between the phases. This has been achieved by performing an instantaneous pressure relaxation at each time step, as described by Saurel and Abgrall [14]. The present case was simpler, however, since the energy equation needed not be accounted for. In short, after the hyperbolic operator has been applied, the volume fraction is modified so as to render the two pressures equal, keeping  $\alpha^{(k)} \rho^{(k)}$  and  $\alpha^{(k)} \rho^{(k)} \mathbf{u}^{(k)}$  constant. This leads to a second-degree

equation with positive solution

$$\alpha^{(\ell)} = \frac{-\psi_2 - \sqrt{\psi_2^2 - 4\psi_1\psi_3}}{2\psi_1}, \quad (79)$$

where

$$\psi_1 = (c^{(\ell)})^2 \rho_o^{(\ell)} - (c^{(g)})^2 \rho_o^{(g)}, \quad (80)$$

$$\psi_2 = -(c^{(\ell)})^2 (\alpha^{(\ell)} \rho^{(\ell)} + \rho_o^{(\ell)}) + (c^{(g)})^2 (-\alpha^{(g)} \rho^{(g)} + \rho_o^{(g)}), \quad (81)$$

and

$$\psi_3 = (c^{(\ell)})^2 \alpha^{(\ell)} \rho^{(\ell)}. \quad (82)$$

The instantaneous pressure relaxation can be thought of as eliminating the volume-fraction equation. The present model is conditionally hyperbolic, whereas the equal-pressure models are dependent upon a suitable choice for the interfacial pressure  $p_{\text{int}}^{(k)}$ , that is, they have more restrictive conditions.

### 3.7 Interfacial-pressure modelling

When the expected number of internal interfaces  $N_{\text{int}}$  in a control volume is larger than 0, the last term of (I) in (65) will tend to drive the velocities and pressures of the two phases together, hence the name ‘relaxation term’. The effect increases with increasing  $N_{\text{int}}$ . In other words,  $N_{\text{int}}$  is a relaxation parameter for both velocity and pressure, such that a large  $N_{\text{int}}$  will cause equality of pressure and no slip (relative velocity) between the phases. This is so because the present model is purely one-dimensional: Fluid particles moving in only one dimension cannot pass each other. The ‘conventional’ multiphase model has been averaged over a control volume (or cross-section) and is therefore able to account for some two-dimensional phenomena, such as slip. A similar cross-sectional averaging could be performed for the present model. However, the calculations would be tedious and are outside the scope of the present paper. Instead, we introduce these ‘two-dimensional’ effects in a more simplistic manner, as described in the following, by setting  $N_{\text{int}} = 0$  and by modifying the expression for  $p^*$ .

### 3.7.1 Standard $p^*$

A simple and linearized solution to the Riemann problem is given by the acoustic solver, or ‘primitive variable Riemann solver (PVRs)’ [17, Section 9.3]. The expression for the ‘star value’ of the pressure (see Figure 2 on page 18) is

$$p^* = \frac{1}{a_l + a_r} [a_r p_l + a_l p_r + a_l a_r (u_l - u_r)], \quad (83)$$

where  $a \equiv \rho c$  can be called the acoustic impedance and the subscripts ‘l’ and ‘r’ denote the left-hand and right-hand states, respectively. This expression will be referred to as the ‘standard  $p^*$ ’.

### 3.7.2 CATHARE model for $p^*$

In the CATHARE code, the following expression was employed for non-stratified flows ‘simply to provide the hyperbolicity of the system’ [3]:

$$p^{(g)} - p_{\text{int}}^{(g)} = p^{(\ell)} - p_{\text{int}}^{(\ell)} = \gamma \frac{\alpha^{(g)} \alpha^{(\ell)} \rho^{(g)} \rho^{(\ell)}}{\alpha^{(g)} \rho^{(\ell)} + \alpha^{(\ell)} \rho^{(g)}} (u^{(g)} - u^{(\ell)})^2. \quad (84)$$

In Bestion [3], the factor  $\gamma$  does not appear explicitly. Evje and Flåtten [6] took  $\gamma = 1.2$ .

Even though it might be difficult to derive the above expression in a rigorous way, we propose setting

$$p^* = p - \gamma \frac{\alpha^{(g)} \alpha^{(\ell)} \rho^{(g)} \rho^{(\ell)}}{\alpha^{(g)} \rho^{(\ell)} + \alpha^{(\ell)} \rho^{(g)}} (u^{(g)} - u^{(\ell)})^2, \quad (85)$$

with  $\gamma = 1.2$  in the gas-liquid Riemann problems.

### 3.7.3 The 0 model for $p^*$

It is often beneficial to take a simple model when the applicability of more complex models is unknown or difficult to evaluate. Consider the following simple model for the interfacial pressure:

$$p^{(k)} - p_{\text{int}}^{(k)} = 0. \quad (86)$$

It is not in widespread use, however, for it yields complex eigenvalues in the four-equation equal-pressure model. The present model, on the other hand, does not, a priori, share this problem. Instead of the expression (85), one may take

$$p^* = \frac{1}{2} (p^{(\ell)} + p^{(g)}) = p, \quad (87)$$

where the last equality stems from the fact that we use instantaneous pressure relaxation in the present work.

#### 4 Reference method

To verify the numerical results obtained using the discrete-equation model, we will compare them with those of an independent numerical method, the ‘Roe5’ scheme, presented in Munkejord [11]. That scheme is based on the continuous multiphase equations and instantaneous pressure relaxation, and it uses a Roe-type Riemann solver.

Some care has to be taken when seeking to compare the results obtained using the standard  $p^*$  model (83) with those of a continuous model. It is necessary to provide the continuous model with interface-models corresponding to the ones of the discrete model in the limit of a fine grid. The continuous limit of the discrete-equation model has been studied by Papin [13, Part II, Chapter 3] in two spatial dimensions, for Riemann solvers whose ‘star values’ can be written in the form

$$p^* = \frac{1}{a_1 + a_2} [a_1 p_2 + a_2 p_1 + a_1 a_2 (u_2 - u_1)], \quad (88)$$

and

$$u^* = \frac{1}{a_1 + a_2} [a_1 u_1 + a_2 u_2 + p_2 - p_1], \quad (89)$$

for some choice of  $a_1$  and  $a_2$ . Among the Riemann solvers fitting into the above scheme are the acoustic solver, the HLLC solver, and the relaxation solver [13].

Here we present the limit expressions for 1D, and the case of no surface tension. The interfacial pressure is

$$p_{\text{int}}^{(\text{g})} = p_{\text{int}}^{(\ell)} = \frac{1}{a^{(\text{g})} + a^{(\ell)}} [a^{(\text{g})} p^{(\ell)} + a^{(\ell)} p^{(\text{g})} + a^{(\ell)} a^{(\text{g})} (u^{(\ell)} - u^{(\text{g})}) \text{sgn}(\partial \alpha^{(\text{g})} / \partial x)], \quad (90)$$

whereas the interfacial velocity is given by

$$u_{\text{int}}^{(\text{g})} = u_{\text{int}}^{(\ell)} = \frac{1}{a^{(\text{g})} + a^{(\ell)}} [a^{(\text{g})} u^{(\text{g})} + a^{(\ell)} u^{(\ell)} + (p^{(\ell)} - p^{(\text{g})}) \text{sgn}(\partial \alpha^{(\text{g})} / \partial x)]. \quad (91)$$

Here we take  $a$  to be the acoustic impedance, and the above expressions are equal to those for the ‘star values’ of the acoustic solver, except for the appearance of the sign function.

Table 1  
Parameters used in the shock tube test problems.

Quantity	Value	Unit
CFL number, $\mu$	0.9	-
Liquid speed of sound, $c^{(\ell)}$	1000	m/s
Gas speed of sound, $c^{(g)}$	$\sqrt{10^5}$	m/s
Liquid reference density, $\rho_o^{(\ell)}$	999.9	kg/m <sup>3</sup>
Gas reference density, $\rho_o^{(g)}$	0	kg/m <sup>3</sup>
Number of interfaces per control volume, $N_{\text{int}}$	0	-

In the following, results from the Roe5 scheme will be shown together with the present results for comparison.

## 5 Test calculations

Here we consider the two two-phase shock-tube problems investigated by Evje and Flåtten [6]. They consist of a 100 m long tube, where the initial state is constant in each half. These test problems enable the investigation of various properties of the numerical scheme. However, it is difficult to envisage a laboratory setup that might realize them.

The employed parameters are given in Table 1. The values for the speed of sound and reference density used in the equation of state are equivalent to the ones used by Evje and Flåtten [6]. The calculations have been performed using the acoustic Riemann solver, our second-order scheme and the van Leer slope-limiter function. The Courant-Friedrichs-Lewy (CFL) number is defined by

$$\mu = \frac{\Delta t}{\Delta x} \max_{\forall k, \forall i} (|u_i^{(k),*}| + c_i^{(k)}). \quad (92)$$

### 5.1 Shock tube problem 1

This problem was introduced by Cortes *et al.* [4]. The initial states can be found in Table 2 on the following page.

Table 2  
Initial states in Shock tube problem 1.

Quantity	Left value	Right value	Unit
Liquid volume fraction, $\alpha^{(\ell)}$	0.71	0.70	-
Liquid velocity, $u^{(\ell)}$	1.0	1.0	m/s
Gas velocity, $u^{(g)}$	65	50	m/s
Liquid density, $\rho^{(\ell)}$	1000.165	1000.165	kg/m <sup>3</sup>
Gas density, $\rho^{(g)}$	2.65	2.65	kg/m <sup>3</sup>
Pressures, $p^{(\ell)} = p^{(g)}$	$2.65 \cdot 10^5$	$2.65 \cdot 10^5$	Pa

### 5.1.1 Standard $p^*$

The results are plotted in Figure 4 on the next page at time  $t = 0.1$  s. Here, the ‘standard’ expression (83) for  $p^*$  has been employed. The graph of the liquid volume fraction in Figure 4(a) is focused on the middle of the tube, where differences between the grids appear more clearly.

Compared to the results of Evje and Flåtten [6] (see also Subsection 5.1.2), some differences can be seen:

- The present method has less numerical diffusion (see e.g. the gas-velocity profile for the 100-cell grid).
- There is an instability at  $x = 50$  m in the liquid velocity plot, Figure 4(c) on the following page.
- The ‘plateaux’ in the velocities are somewhat different.
- The jump in pressure at  $x = 50$  m is larger in the present case, and contrary to the case of Evje and Flåtten [6], the highest pressure is on the left-hand side.

Figure 4 also shows results obtained using the Roe5 method on an equidistant grid with a grid spacing,  $\Delta x$ , equal to that of the 10000-cell grid of the discrete-equation model. The employed interfacial closures were the ones in Equations (90)–(91). It is clear that the discrete-equation model and the Roe5 method give the same solution for fine grids.

### 5.1.2 CATHARE model for $p^*$

The case of the previous subsection has been recalculated employing the CATHARE model (85) for  $p^*$ . The results are shown in Figure 5 on page 27. The clearest difference from the preceding case, is that the pressure jump at  $x = 50$  m is much smaller. Moreover, the plateaux in the velocities and in the pressure are straight, and in the case of the gas velocity, the levels

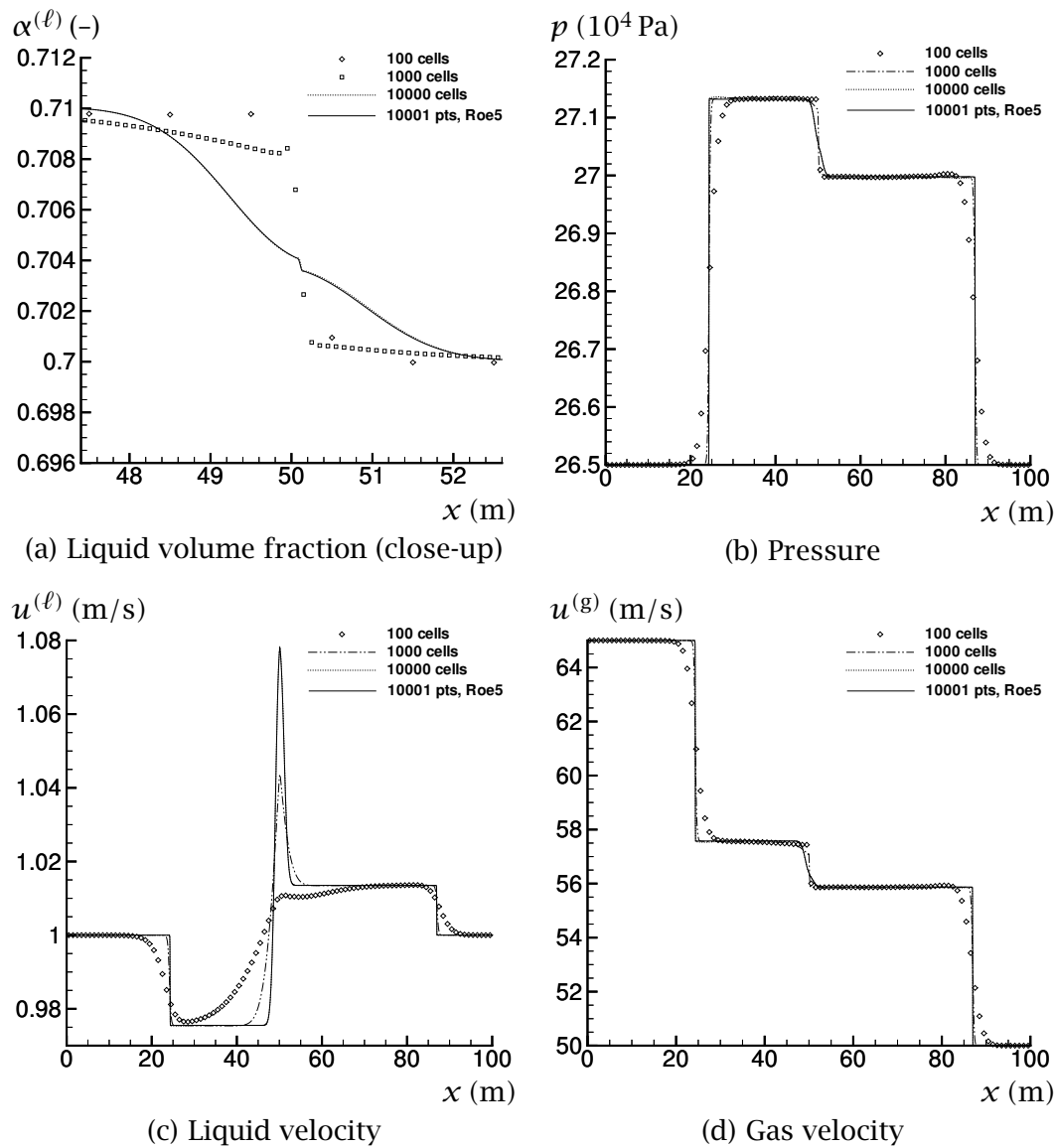


Figure 4. Shock tube problem 1, calculated using the ‘standard’  $p^*$ .  
of the middle plateaux are slightly higher.

Figure 5 shows very close agreement between the present model and the Roe5 scheme.

### 5.1.3 The 0 model for $p^*$

Results for the 0 model (87) are plotted in Figure 6 on page 28. As can be observed, they are similar to the results in Figure 5 obtained using the CATHARE model, except that the 0 model yields an undershoot in all variables at  $x = 50$  m, particularly in the liquid volume fraction and in the liquid velocity. Furthermore, the undershoot increases with grid re-

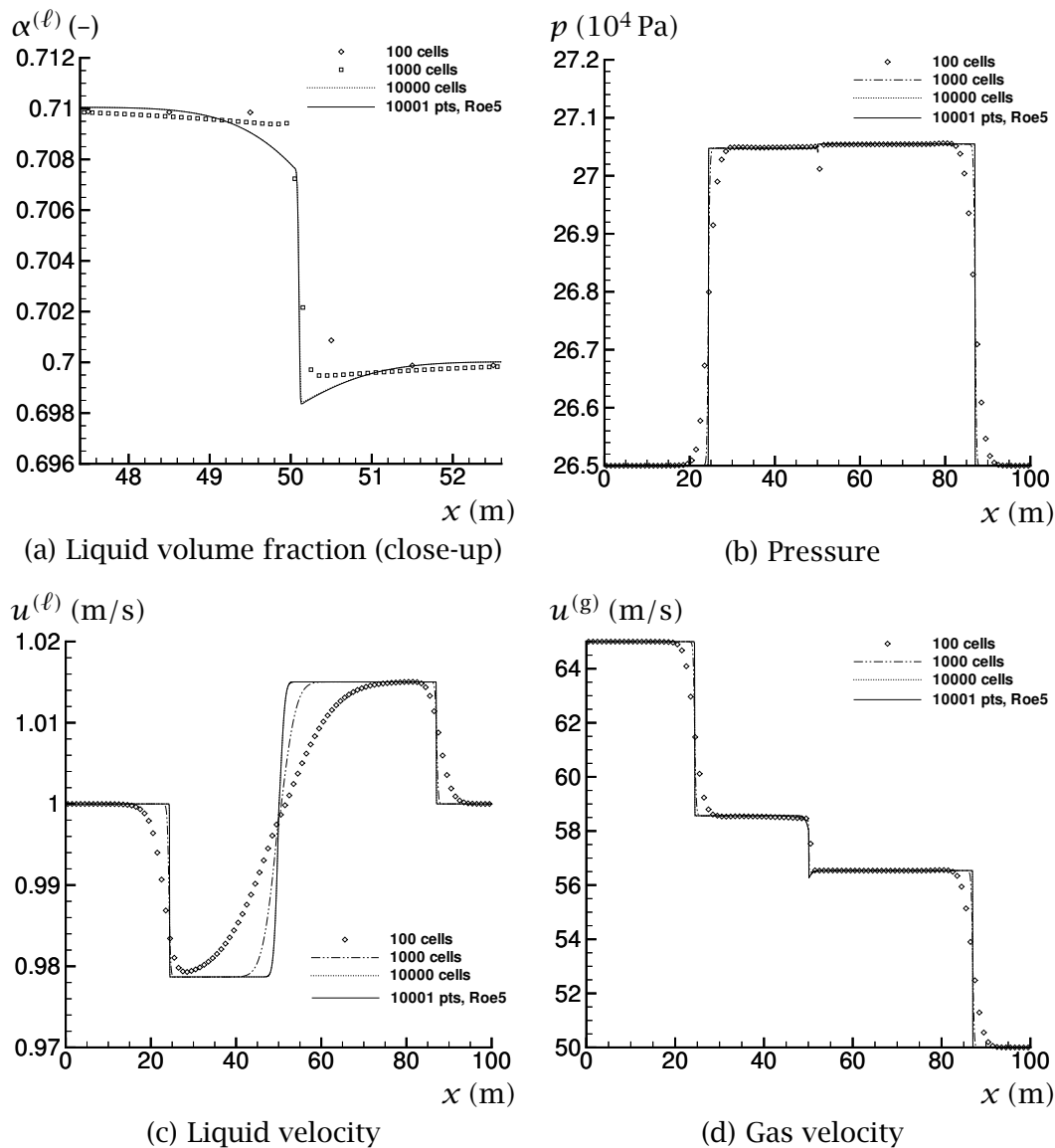


Figure 5. Shock tube problem 1, calculated using the CATHARE model for  $p^*$ .

finement. The results agree closely with those of the Roe5 scheme, which, indeed, also displays undershoots at  $x = 50$  m. This behaviour might be a result of the complex eigenvalues of the ‘underlying’ one-pressure four-equation two-phase model.

## 5.2 Shock tube problem 2

The second shock tube problem features a liquid velocity jump, as well as a larger jump in the volume fraction. The initial states are displayed in Table 3 on the next page.

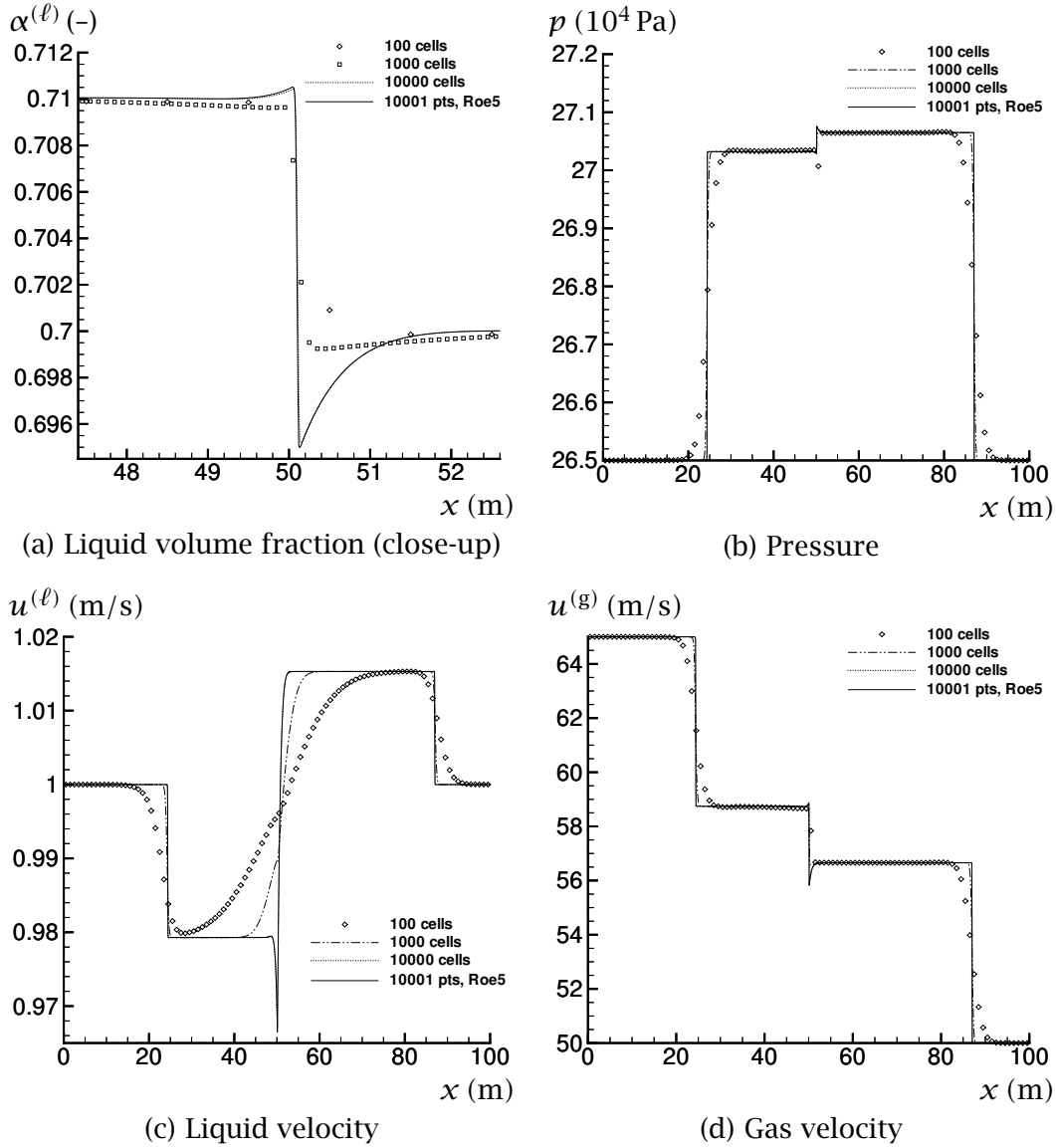


Figure 6. Shock tube problem 1, calculated using the 0 model for  $p^*$ .

Table 3

Initial states in Shock tube problem 2.

Quantity	Left value	Right value	Unit
Liquid volume fraction, $\alpha^{(\ell)}$	0.70	0.10	-
Liquid velocity, $u^{(\ell)}$	10	15	m/s
Gas velocity, $u^{(g)}$	65	50	m/s
Liquid density, $\rho^{(\ell)}$	1000.165	1000.165	kg/m <sup>3</sup>
Gas density, $\rho^{(g)}$	2.65	2.65	kg/m <sup>3</sup>
Pressures, $p^{(\ell)} = p^{(g)}$	$2.65 \cdot 10^5$	$2.65 \cdot 10^5$	Pa

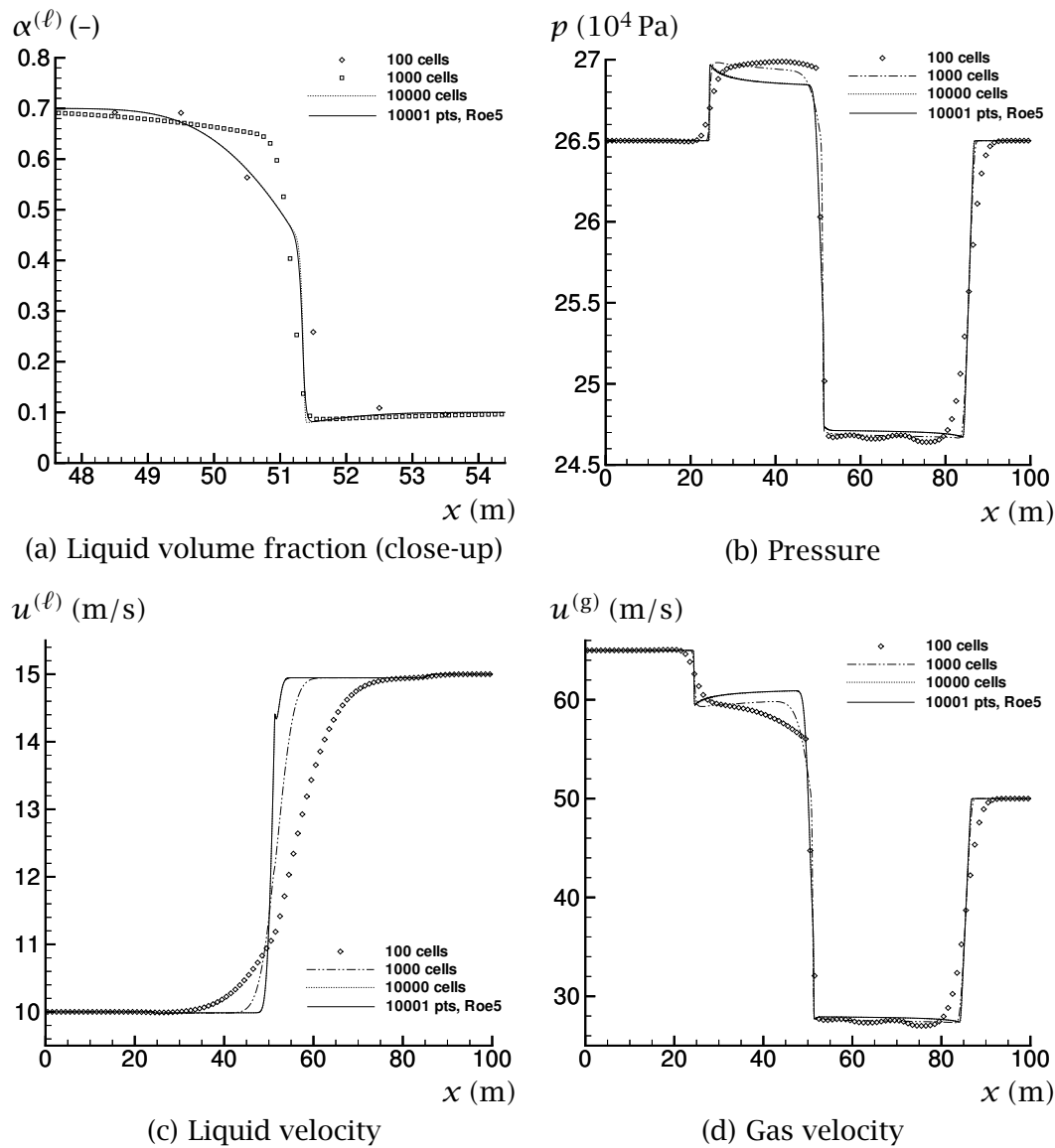


Figure 7. Shock tube problem 2, calculated using the 'standard'  $p^*$ .

### 5.2.1 Standard $p^*$

Numerical results for the 'standard' expression for  $p^*$  are shown in Figure 7. Again, the calculations performed using the discrete-equation model agree very well with those of the Roe5 scheme. However, the pressure and gas-velocity profiles are quite different from those of Evje and Flåtten [6]. This has numerical, but above all, modelling reasons, as can be seen by comparing with the results obtained using the CATHARE interfacial-pressure model in Subsection 5.2.2.

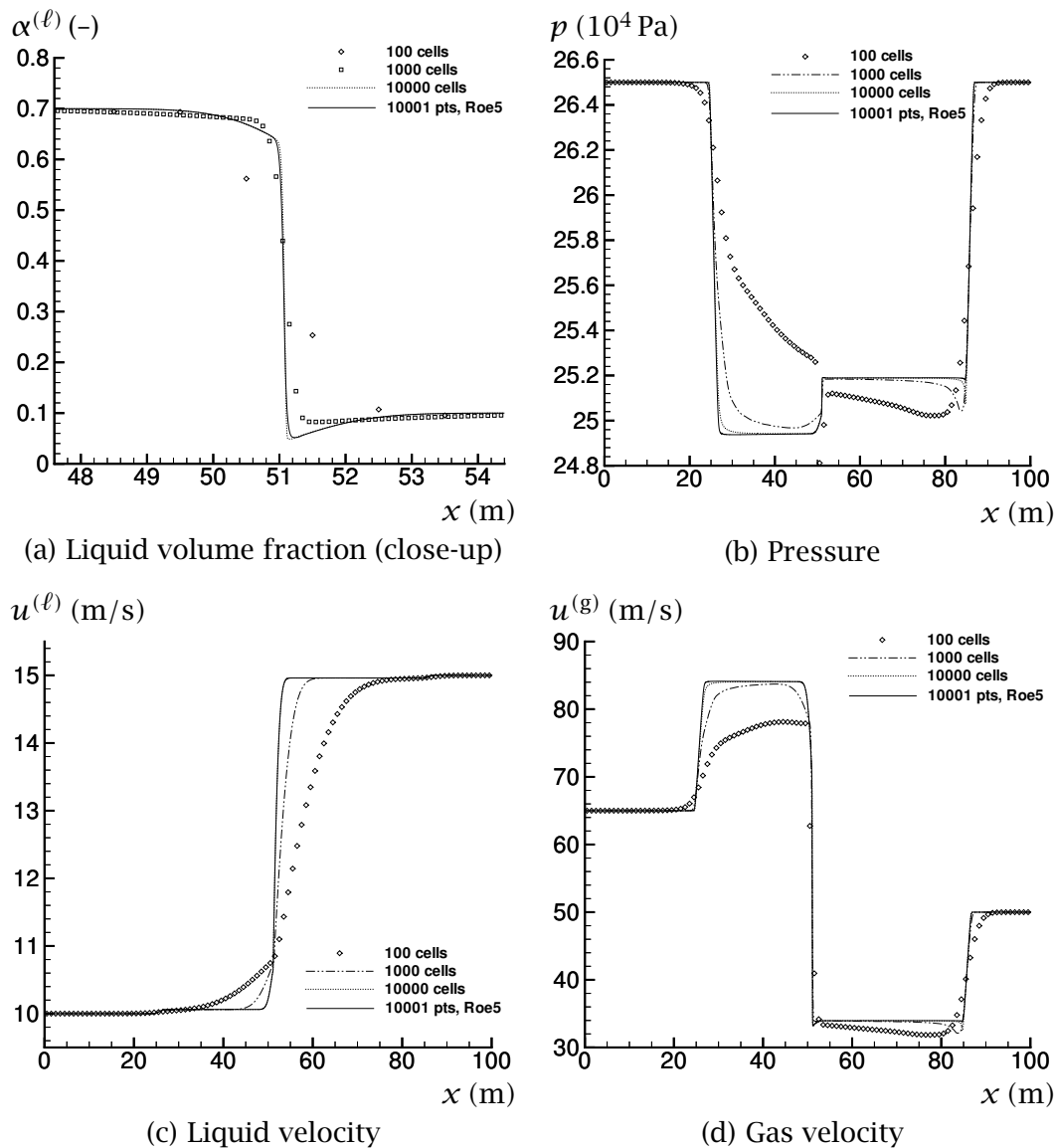


Figure 8. Shock tube problem 2, calculated using the CATHARE model for  $p^*$ .

### 5.2.2 CATHARE model for $p^*$

The results for the CATHARE model for  $p^*$  are given in Figure 8. The fine-grid results are quite similar to those of Evje and Flåtten [6].

Comparing with the results obtained using the standard  $p^*$  in Figure 7 reveals that the main differences occur for the pressure (Figures 8(b) and 7(b)) and the gas velocity (Figures 8(d) and 7(d)), where the plateaux in the middle section of the tube are on different levels. For the CATHARE model, the pressure in the tube is nowhere higher than the initial value of  $26.5 \cdot 10^4$  Pa. For the standard  $p^*$  model, on the other hand, the pressure in the middle-left section is  $27 \cdot 10^4$  Pa. The situation for the gas velocity is reversed: It is for the CATHARE model that gas velocities occur which

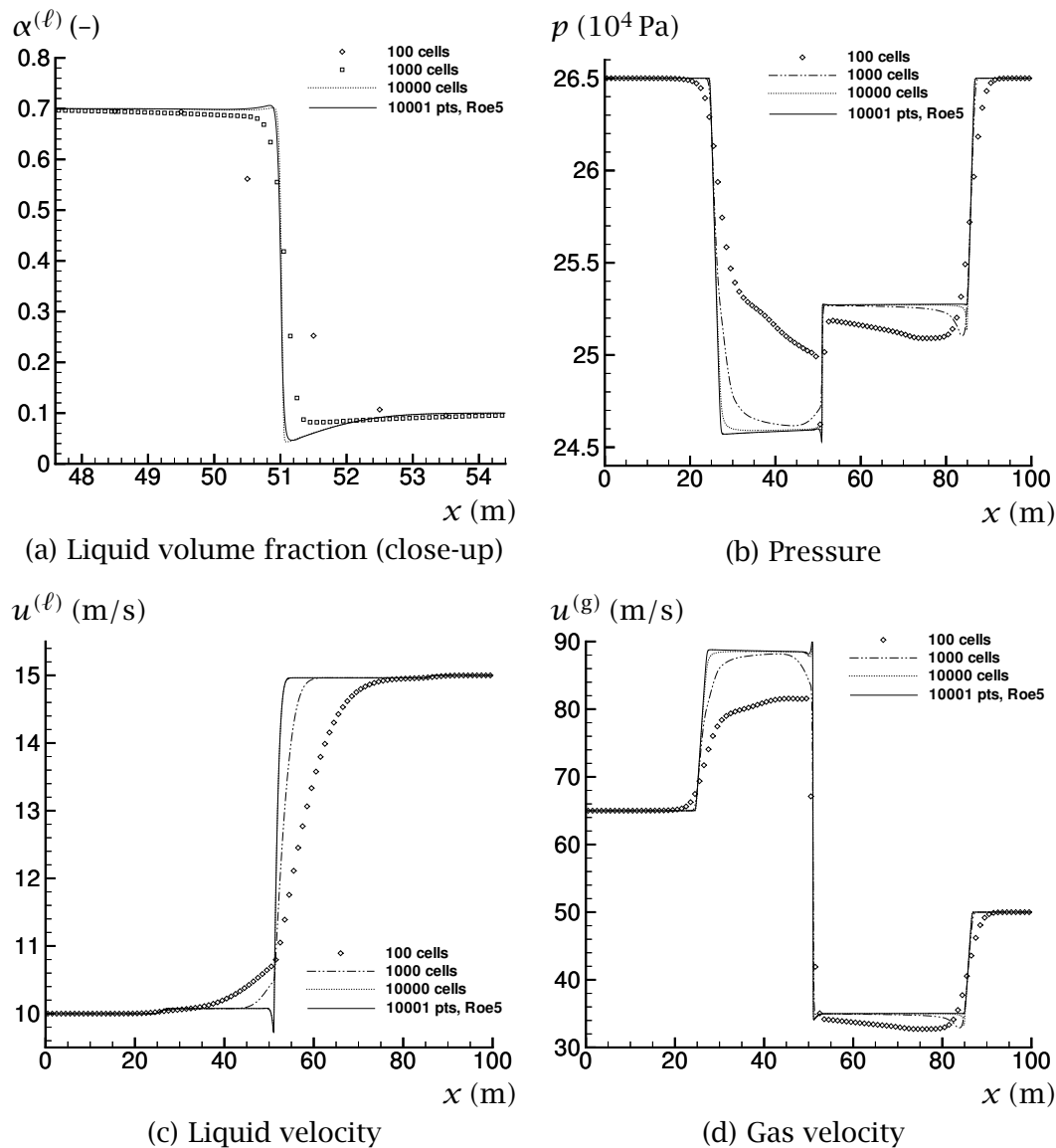


Figure 9. Shock tube problem 2, calculated using the 0 model for  $p^*$ .

are higher than the initial value.

These differences are a result of the interfacial closure models, and therefore it would have been interesting to be able to compare the calculations to experimental data.

### 5.2.3 The 0 model for $p^*$

Figure 9 shows the results obtained using the 0 model (87) for  $p^*$ . Like in the case of Shock tube 1, the results are similar to those of the CATHARE model for  $p^*$ . There are some differences, however: The pressure plateau to the left of  $x = 50$  m (Figure 9(b)) is lower than that of Figure 8(b), so

that the pressure jump at  $x = 50$  m is higher. Further, the plateau in the gas velocity to the left of the middle of the tube in Figure 9(d) is higher than that in Figure 8(d).

The plots for the 0 model in Figure 9 have more under- and overshoots than those for the CATHARE model in Figure 8, but this is somewhat less noticeable than for Shock tube 1 (Figures 6 and 5).

## 6 Conclusions

We have presented a five-equation isentropic version of the discrete seven-equation two-phase model of Abgrall and Saurel [1]. In the discrete-equation model, Riemann problems are solved between pure fluids. Hence, the difficulty of non-conservative products is avoided while solving the Riemann problem. Another characteristic of the discrete-equation model is that the properties of the Riemann solver influence the phasic interaction.

We have shown how different interfacial-pressure expressions can be incorporated into the discrete-equation models. One example is the CATHARE expression, often cited in the literature.

Two shock-tube problems from the literature [6] have been considered. The numerical results were strongly dependent on the employed expression for the interfacial pressure. The convergence properties of the scheme were also affected.

When the CATHARE interfacial-pressure model was employed, our results were similar to those presented by Evje and Flåtten [6].

The correspondence between the discrete-equation model and the ‘conventional’ continuous model has been discussed. Continuous-limit expressions for the interfacial pressure and velocity were given for the discrete model. These expressions were employed in the Roe5 scheme [11], a continuous model. Very good agreement between the discrete-equation model and the Roe5 scheme was obtained.

## Acknowledgements

The first author has received a doctoral fellowship and an overseas fellowship from the Research Council of Norway, and has had a one-semester

stay at Mathématiques Appliquées de Bordeaux (MAB).

The second author has received a PhD grant from the Commissariat à l'Énergie Atomique of France and wishes to thank F. Coquel, Q. H. Tran and N. Seguin for the interesting reflections at CEMRACS 2003 concerning the system of equations considered here.

The authors are grateful to Rémi Abgrall at MAB for the fruitful discussions during the preparation of the paper.

Thanks are due to Vincent Perrier at Mathématiques Appliquées de Bordeaux, and to Erik B. Hansen at NTNU.

The careful review of the referees is also acknowledged.

## References

- [1] Abgrall R., Saurel R. Discrete equations for physical and numerical compressible multiphase mixtures. *J. Comput. Phys.* 186 (2) (2003) 361–396.
- [2] Andrianov N., Warnecke G. The Riemann problem for the Baer-Nunziato two-phase flow model. *J. Comput. Phys.* 195 (2) (2004) 434–464.
- [3] Bestion D. The physical closure laws in the CATHARE code. *Nucl. Eng. Design* 124 (3) (1990) 229–245.
- [4] Cortes J., Debussche A., Toumi I. A density perturbation method to study the eigenstructure of two-phase flow equation systems. *J. Comput. Phys.* 147 (2) (1998) 463–484.
- [5] Drew D.A., Passman S.L. *Theory of Multicomponent Fluids*, vol. 135 of *Applied Mathematical Sciences*. Springer-Verlag, New York, 1999.
- [6] Eyje S., Flåtten T. Hybrid flux-splitting schemes for a common two-fluid model. *J. Comput. Phys.* 192 (1) (2003) 175–210.
- [7] Karni S., *et al.* Compressible two-phase flows by central and upwind schemes. *ESAIM - Math. Model. Num.* 38 (3) (2004) 477–493.
- [8] Le Métayer O., Massoni J., Saurel R. Modelling evaporation fronts with reactive Riemann solvers. *J. Comput. Phys.* 205 (2) (2005) 567–610.
- [9] LeVeque R.J. *Numerical Methods for Conservation Laws*. Lectures in Mathematics, ETH Zürich, Birkhäuser Verlag, Basel, Switzerland, 1990.
- [10] LeVeque R.J. *Finite Volume Methods for Hyperbolic Problems*. Cambridge University Press, Cambridge, UK, 2002.
- [11] Munkejord S.T. *Analysis of the two-fluid model and the drift-flux model for numerical calculation of two-phase flow*. Doctoral thesis,

- Norwegian University of Science and Technology, Department of Energy and Process Engineering, Trondheim, 2005. In progress.
- [12] Niu Y.Y. Advection upwinding splitting method to solve a compressible two-fluid model. *Int. J. Numer. Meth. Fl.* 36 (3) (2001) 351–371.
  - [13] Papin M. *Contribution à la modélisation d'écoulements hypersoniques particuliers. Étude et validation d'un modèle diphasique discret.* Thèse, Université Bordeaux 1, Mathématiques Appliquées, France, 2005.
  - [14] Saurel R., Abgrall R. A multiphase Godunov method for compressible multifluid and multiphase flow. *J. Comput. Phys.* 150 (2) (1999) 425–467.
  - [15] Saurel R., LeMetayer O. A multiphase model for compressible flows with interfaces, shocks, detonation waves and cavitation. *J. Fluid Mech.* 431 (2001) 239–271.
  - [16] Slattery J.C. Flow of viscoelastic fluids through porous media. *AIChE J.* 13 (6) (1967) 1066–1071.
  - [17] Toro E.F. *Riemann solvers and numerical methods for fluid dynamics.* Springer-Verlag, Berlin, second edn., 1999.
  - [18] van Leer B. On the relation between the upwind-differencing schemes of Godunov, Engquist-Osher and Roe. *SIAM J. Sci. Stat. Comp.* 5 (1) (1984) 1–20.
  - [19] Whitaker S. Advances in theory of fluid motion in porous media. *Ind. Eng. Chem.* 61 (4) (1969) 14–28.